Indoor High-precise Three-dimensional Positioning Algorithm Based on Visible Light Communication and Fingerprinting Using K-Means and Random Forest

Jiajia Jiang[3], Weipeng Guan [1、2]*, Zhounan Chen[2], Yirong Chen[3]

（*1. School of Materials Science and Engineering, South China University of Technology, Guangzhou, Guangdong 510640, China*

2. School of Automation Science and Engineering, South China University of Technology, Guangzhou, Guangdong 510640, China

3.School of Electronic and Information Engineering, South China University of Technology, Guangzhou, Guangdong 510640, China）

Corresponding author. Email: * gwpscut@163.com or augwpscut@mail.scut.edu.cn

Abstract: Recently, visible light communication (VLC) has been widely used in indoor positioning. Considering that conventional VLC-based positioning (VLP) algorithms are susceptible to interference and can not adapt well to the complex indoor location environment, this paper proposes an high-precise indoor three-dimensional positioning algorithm based on VLC and fingerprinting using fusion of K-Means (KM) and Radom Forest (RF) algorithm. Unlike the trilateration techniques based on received signal strength (RSS), the mentioned system does not depend on the model parameters and is robust to external interference. Besides, the proposed system introduces the concept of VLP kernel to compress the fingerprint database and shorten the training time. And we have validated the feasibility of our proposed VLC-based positioning system using fingerprinting in the real indoor VLP environment. Both simulation and experiment results verify that our proposed algorithm delivers satisfactory performance in terms of real-time ability and positioning accuracy, both of which are crucial for the performance of indoor positioning system. Therefore, our proposed positioning system with strong interference immunity is a promising candidate for future indoor positioning applications.

Keywords: visible light communication (VLC); VLC-based positioning (VLP); fingerprinting; K-Means and Radom Forest Algorithm; high-precise indoor three-dimensional positioning; positioning accuracy

1 Introduction

Nowadays, indoor localization technology for mobile devices is widely applied to large-scale indoor occasions, such as parking lots, museums, shopping malls and so on. It is fundamental for the tracking for mobile intelligent devices and navigation service. Though the global positioning system (GPS) has achieved precise outdoor localization, it is usually unavailable to indoor environments where signals from satellites are strongly attenuated or affected by multipath propagation. Conventional indoor positioning techniques include wireless local area network (WLAN), Zig Bee, Ultra Wideband (UWB), Bluetooth, Radio-frequency Identification (RFID), Infrared Ray and Ultrasonic Wave. However, these techniques suffer from deficiencies such as requiring additional infrastructure, low accuracy, electromagnetic interference, low security, and high time cost [1]-[4]. Different from the traditional indoor positioning technologies mentioned above, VLP technology is an eco-friendly and efficient indoor positioning technology based on visible light communication technology [5]-[7]. Compared with the previous indoor positioning techniques, it has the following advantages: firstly, VLP system utilizes the existing lighting facilities to realize lighting and positioning simultaneously, which is cost-saving and environmentally friendly. Secondly, VLP can be applied in environments like hospitals and airplanes without generating RF interference, where RF is hazardous or even forbidden. Therefore, indoor VLP systems have recently gained popularity as effective alternatives to the traditional techniques [8]. At present, for the photodiode-based VLP systems, triangulation is used to determine the absolute position of terminal by using the geometric properties of triangles, which involves the time of arrival (TOA), the time difference of arrival (TDOA), RSS, and angle of arrival (AOA). Among the above techniques, RSS based positioning is

preferred due to its low cost and high accuracy, and it works out the distance between LED and terminal based on the strength of received signal strength [9]. However, the problem of inter-cell interference must be solved when measuring received light signal strength of multiple LEDs. So in [10]-[13], to reduce inter-cell interference, the visible light from LEDs has been modulated with code division multiple access (CDMA) technology to separate the overlapping signals in time domain and frequency domain.

Over the last decade, great effort has been dedicated to develop efficient, accurate, and robust algorithms for VLP problems. So far, Three-dimensional VLP has been extensively explored. In [14], Huanhuan Zheng et al. determined the receiver's coordinates using the original 2-D positioning algorithm improved by an error correcting algorithm for the corners, which is developed into a 3-D positioning algorithm. In [15], Ye Cai et al. transformed the VLP problem into a global optimization problem and use a modified particle swarm optimization algorithm to solve it with an average error of 3.9 mm. In [16], Wu adopted a 3-D positioning strategy by calculating the overlapped area between three circles on the projection plane based on differential evolution algorithm, which achieved an average accuracy of 0.69cm with an average positioning speed of 24.26ms. However, the systems mentioned above are mainly based on the basic triangulation methods or propagation models to realize positioning, which often produce large positioning error owing to the complex indoor optical channel environment. When the indoor environment changes, the signal propagation model will fail to characterize the mapping relationship between RSS and distance, so it is no longer applicable for precise positioning. Therefore, researchers turns to explore visible light fingerprinting-based location schemes [17]. As indoor RSS value decreases with the propagation distance, RSS can be used as the environmental feature to match with indoor location and finally realize positioning. The indoor location method based on RSS fingerprint can be divided into two stages: off-line sampling stage and on-line location stage. Chin-Wei Hsu et al. [18] utilized second order polynomial hypothesis function of the estimated position coordination according to the received power, and

applied machine learning algorithm to correct the parameters of the hypothesis function through iteration. However, it can only achieve two-dimensional positioning within a certain height range, and can not work out the height of the target, so it can not satisfy the needs of three-dimensional positioning. Xu [19] proposed a VLC-based 3-D positioning system using fingerprinting and K-Nearest neighbor. But this method requires to calculate the distance between each RSS fingerprint and observed RSS, thereby leading to a large amount of computation and poor real-time performance. In [20], Xiansheng Guo et al. proposed a multiple classifiers fusion fingerprint localization framework based on multiple machine learning approaches, which achieved accurate and robust VLC indoor localization. However, it is impractical to combine too many algorithms simultaneously in real real-time positioning process.

In this paper, we innovatively put forwards an high-precise indoor three-dimensional positioning system based on visible light communication and fingerprinting using fusion of K-Means (KM) and Radom Forest (RF) algorithm, which does not need to estimate the measured triangulation value accurately and is reliable in complex multipath propagation. Unlike the trilateration techniques based on the RSSs, the mentioned system does not depend on the model parameters and shows strong interference immunity. K-Means algorithm [21] is a simple traditional algorithm for solving clustering problems, so we choose it to cluster the fingerprint database objects for simplifying the fingerprint database. In KM algorithm, the data objects in the database are divided into K clusters iteratively until the similarity of objects in the same cluster is high enough. Radom Forest Algorithm is an effective machine learning technique. RF is a group of decision trees trained independently on a random selection of features, which have been shown to be effective in processing a lot of classification and regression problems [22]–[23]. Therefore, the proposed system can deliver satisfactory performance in terms of real-time ability and positioning accuracy, both of which are crucial for the performance of indoor positioning system.

The remainder of this paper is organized as follows. Section 2 describes the indoor optical wireless channel model and provides details of the proposed fusion of K-Means and Random Forest algorithm using fingerprint for VLP. Section 3 and Section 4 describe the results and analysis of simulation and experiment to verify the proposed system. Section 5 gives the conclusion of the article.

2 System Principle and Algorithm

2.1 Indoor Optical Wireless Channel Model

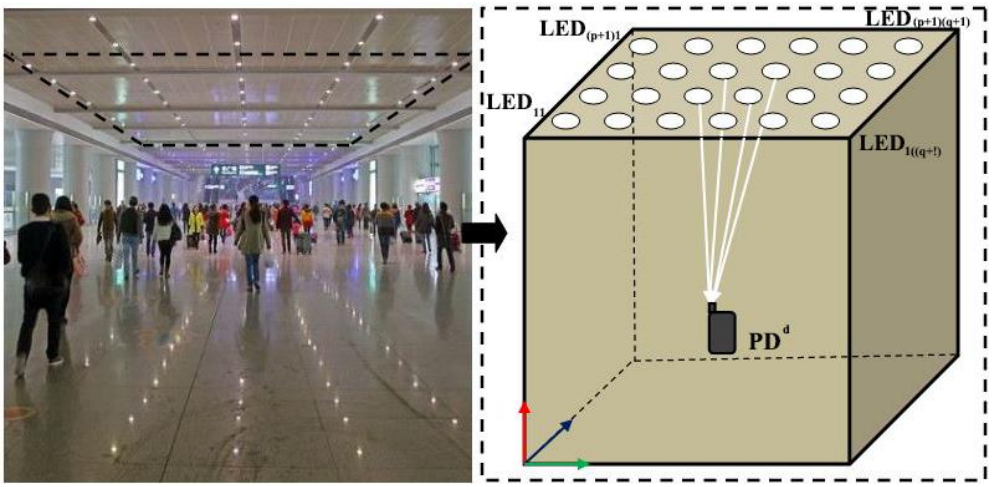

Fig. 1. Indoor optical wireless positioning system.

As shown in Fig. 1, the proposed VLP system is applied in an indoor environment with a large number of LEDs mounted on the ceiling to satisfy the requirement of lighting. Photodiode(PD) receivers are installed on indoor intelligent terminals to be localized such as smart mobile phones and robots to receive signals from LEDs. The position coordinate of LED_{ij} can be labeled as (X_{ij}, Y_{ij}, Z_{ij}), where i=1,2,3,...,p+1 and j=1,2,3,...,q+1. Here, i and j represent the LED distribution number of rows and columns, respectively. Similarly, the coordinates of different PDs, PD^d, can be labeled as (x^d, y^d, z^d), (d=1,2,3,... is the identifier of sampling points (SPs)), respectively. Generally, the radiant intensity of a LED is assumed to follow a Lambertian radiation pattern due to its large

beam divergence. So the received optical power of the PD located at (x^d, y^d, z^d) from the LED located at (X_{ij}, Y_{ij}, Z_{ij}) can be given as [24]:

$$P_{ij}^d = P_{ij}^e \frac{A(m+1)}{2\pi dis_{ij}^d} T(\psi_{ij}^d) G(\psi_{ij}^d) cos^m(\varphi_{ij}^d) cos^M(\psi_{ij}^d) \quad (1)$$

where P_{ij}^e is the emitted optical power of LED_{ij}; A is the effective area of PD^d; dis_{ij}^d is the distance between LED_{ij} and PD^d; ψ_{ij}^d is the incident angle of PD^d; φ_{ij}^d is the irradiant angle of LED_{ij}; $T(\psi_{ij}^d)$ is the gain of the optical filter; $G(\psi_{ij}^d)$ is the gain of the optical concentrator; the Lambertian parameter $m = \frac{-ln2}{ln(cos(\varphi_{1/2}))}$ and $M = \frac{-ln2}{ln(cos(\psi_{1/2}))}$, where $\varphi_{1/2}$ and $\psi_{1/2}$ are the half-power angle of the LED_{ij} and PD^d, respectively.

According to the geometric model in Fig.3, dis_{ij}^d can be calculated as:

$$dis_{ij}^d = \sqrt{(x^d - X_{ij})^2 + (y^d - Y_{ij})^2 + (z^d - Z_{ij})^2} \quad (2)$$

The irradiant angle φ_{ij}^d can be represented as:

$$cos(\varphi_{ij}^d) = \frac{|z^d - Z_{ij}|}{dis_{ij}^d} \quad (3)$$

Theorically speaking, we can calculate (x^d, y^d, z^d) with Equation (1), (2) and (3), which estimate the distances between transmitters and a PD by using the received RSSs. However, the received RSSs are easily affected by many model parameters mentioned above [25]. So, it is difficult to estimate dis_{ij}^d accurately, which greatly degrades the visible light localization performance. This makes the fingerprint algorithm more suitable for indoor VLP scene, which realizes positioning through matching the location information and the RSS data detected from environment. It takes the noise interference as part of RSS fingerprint, so even in the case where traditional localization system mentioned above fails to characterize the mapping relationship between RSS and distance,

fingerprint localization system can still work reliably. Therefore, the fingerprint localization system has better anti-interference performance than the traditional localization system.

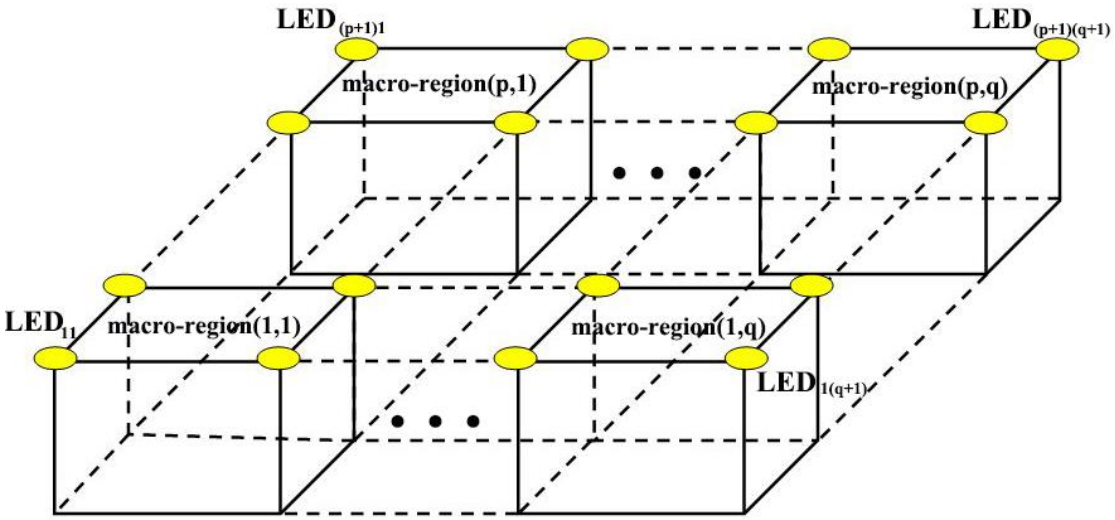

Fig. 2. Macro partition of area in VLC-based positioning using fingerprint.

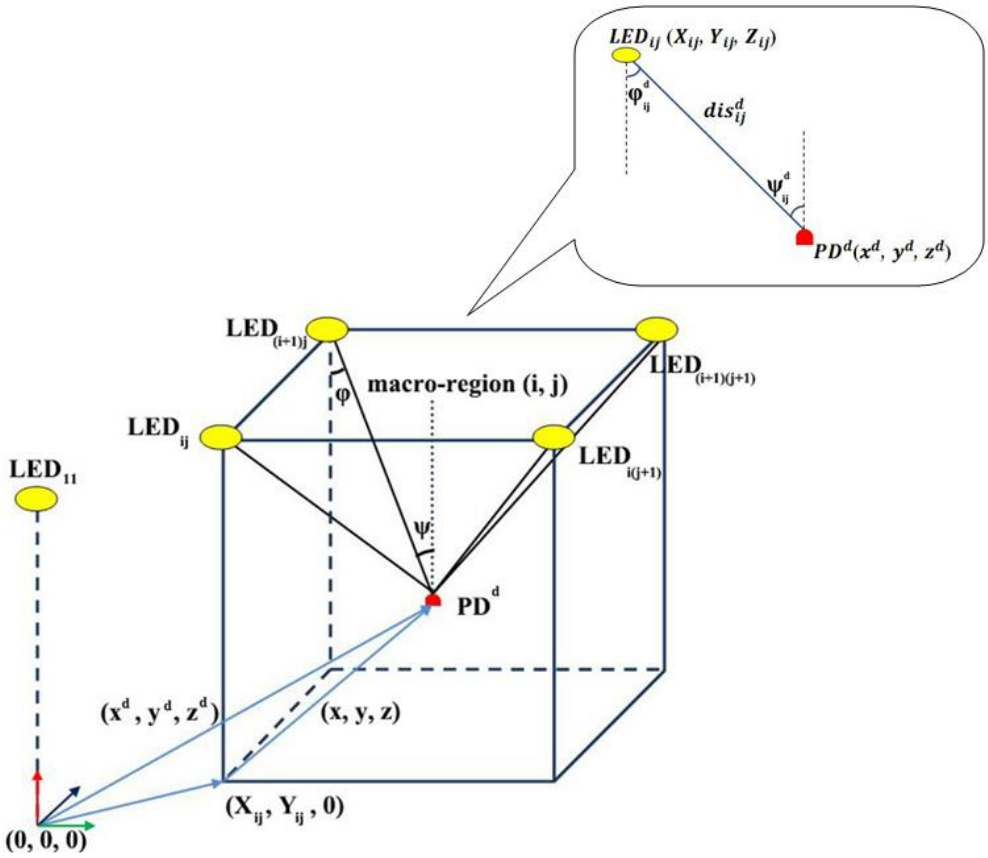

Fig. 3. The scene graphic of indoor VLC-based positioning using fingerprint.

As shown in Fig. 2, $(p+1)\times(q+1)$ LEDs are installed on the ceiling in the position area evenly. PD^d (d=1,2,…,D) are located at D sampling points. The received optical power by PD^d from LED_{ij} is defined as S_{ij}^d. In VLC-based positioning using fingerprint, we collect the fingerprint data from multiple SPs and use them to estimate the coordinates of the measured point. However, when the values of p and q enlarge, the size of the fingerprint database rapidly grows, and many invalid data are generated. For example, there are often cases when $S_{ij}^d = 0$, which do not help positioning but greatly increase computing burden.

To adapt the fingerprint location to scenes with large-scale LEDs, this paper proposes a real-time and high-precise three-dimensional positioning system based on fusion of K-Means and Radom Forest Algorithm. In our proposed system shown in Fig. 3, the absolute positioning is transformed into two steps of relative positioning based on the coordinate transformation theory: (1) get the relative position coordinate of LED_{ij} with respect to LED_{11}; (2) calculate the relative position coordinate of PD^d with respect to LED_{ij}. So we can get the position estimate of PD^d indirectly by:

$$\begin{bmatrix} x^d \\ y^d \\ z^d \end{bmatrix} = \begin{bmatrix} X_{ij} \\ Y_{ij} \\ 0 \end{bmatrix} + \begin{bmatrix} x \\ y \\ z \end{bmatrix} \tag{4}$$

Since all LEDs in the ceilings are coded and transmit information of LED's position coordinates , the PD in receiver can receive them and obtain the coordinate information. Therefore, X_{ij} and Y_{ij} in Equation (4) can be obtained through VLC. And the whole positioning area is divided into $p \times q$ macro-regions, each of which has four LEDs mounted on the four corners. We only need to perform VLC-based positioning using fingerprint in these macro-regions.

2.2 Fusion of K-Means and Random Forest Algorithm Using Fingerprinting for VLP

This paper puts forwards an indoor three-dimensional visible light fingerprint positioning system based on fusion of K-Means (KM) and Random Forest (RF) algorithm, where KM algorithm is used for clustering and RF algorithm is used for reclassification. Our proposed algorithm includes offline training stage and online positioning stage. In training stage, Firstly, K-Means algorithm divides the located macro-region into several non-overlapping sub-regions through clustering fingerprint data, and each sub-region contains SPs with similar RSSs. Secondly, in each sub-region, RF classifier is trained using fingerprints grouped into the corresponding sub-region. In positioning stage, first the KM classifier is used to cluster the observed RSS value from the test point to determine which sub-region it belongs to. Next, the trained RF classifier of the object sub-region carries out a second classifications to the observed value and utilize the output results of decision trees to generate the final position estimate. Figs. 4 and 5 show the training and localization activity diagrams of the proposed system, respectively. In the following, specific steps involved in training and positioning procedures are described in detail.

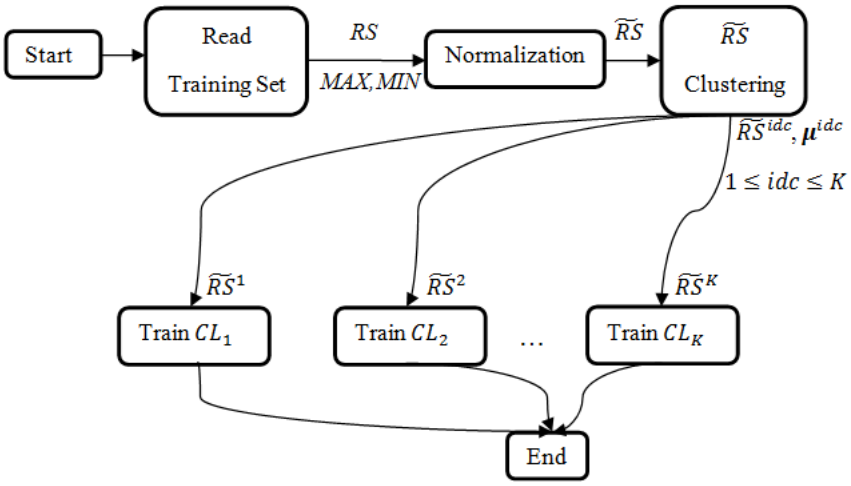

Fig. 4. Training Process.

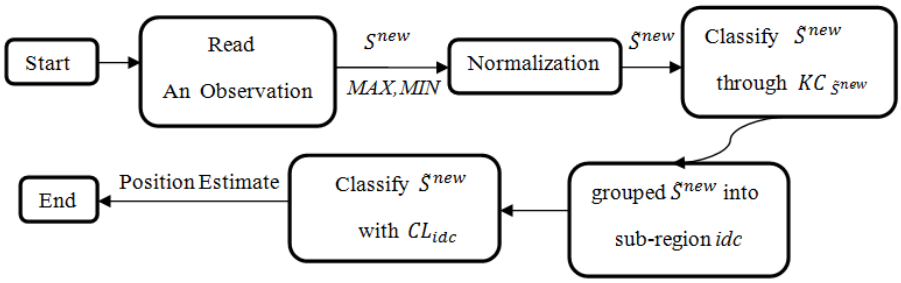

Fig. 5. Positioning Process.

2.3.1 Offline Training: Region Subdivision, Construction of RF and Optimization of Fusion Algorithm Parameters

Since the positioning algorithm in each macro-region is the same, they can be unified and summarized as a fingerprinting-based VLP kernel. We only need to utilize the data of the fingerprinting-based VLP kernel during the training phase. Let $RS = \{ S^1, S^2, S^3, \dots, S^d, \dots, S^D \}$ be a set of 4-dimensional observations in one macro-region, where each element can be described as:

$$S^d = [\, S_{ij}^d \;\; S_{(i+1)j}^d \;\; S_{i(j+1)}^d \;\; S_{(i+1)(j+1)}^d \,] \tag{5}$$

where S^d is the observation vector of received optical power at the d-th SP, S_{ij}^d represents the signal strength emitted by the LED in Line i, Column j for the observation S^d. A 3-dimensional class label (x_d, y_d, z_d) is associated to each observation and it represents the position coordinates related to that acquisition. So the complete fingerprint database can be defined as:

$$\begin{bmatrix} S^1 \\ \dots \\ S^d \\ \dots \\ S^D \end{bmatrix} \leftrightarrow \begin{bmatrix} C^1 \\ \dots \\ C^d \\ \dots \\ C^D \end{bmatrix} \tag{6}$$

where $C^d = [\, x_d \;\; y_d \;\; z_d \,]$, representing three-dimensional coordinates of SPs related to corresponding acquisition of signal strength.

The training set RSS of a macro-region is used to train the proposed fingerprint localization system based on fusion of K-Means and Radom Forest algorithm. Though such a procedure could be time consuming, it only needs to be performed once during the system setup. The training stage can be divided into three steps:

- Data normalization: pre-processing and aiming at extracting a feature vector from each observation;
- Sub-regions definition: dividing the located macro-region into non-overlapping sub-regions featured by similar observation values;
- Training of Radom Forest Classifier: constructing Radom Forests Classification model in each sub-region.

step 1. Data Normalization

The normalized training set $\widetilde{RS} = \{ \tilde{S}^1, \tilde{S}^2, \tilde{S}^3, \dots, \tilde{S}^d, \dots, \tilde{S}^D \}$ is acquired by mapping each training data in the range [0; 1]. This normalization serves for representing the data in a easier-to-manage form. The first step of data normalization is determining, for each receiver, the minimum and maximum value in the training set, so that all the values can successively be normalized in the range [0; 1] accordingly. Let us define $MAX = \{ M_{00}, M_{01}, M_{10}, M_{11} \}$ and $MIN = \{ m_{00}, m_{01}, m_{10}, m_{11} \}$ as the sets of maximum and minimum values observed from each LED in a macro-region over the whole training set RSS respectively. Specifically

$$M_{ab} = \max(S^d_{(i+a)(j+b)}) \tag{7}$$

$$m_{ab} = \min(S^d_{(i+a)(j+b)}) \tag{8}$$

for each $S^d \in \mathrm{RS}$, the normalized value of each single feature $\tilde{S}^d_{(i+a)(j+b)}$, $a = 0, 1;\ \mathrm{b} = 0, 1$ is calculated as follows:

$$\tilde{S}^{d}_{(i+a)(j+b)} = \frac{S^{d}_{(i+a)(j+b)} - m_{ab}}{M_{ab} - m_{ab}} \quad (9)$$

step 2. Sub-region Grouping Based on K-Means Clustering

In each macro-region, the data sets at SPs are composed of a series of normalized feature vectors. The K-Means algorithm is used to divide these feature vectors into several clusters, each of which has a cluster centroid and a number of cluster members. Correspondingly, each macro-region is grouped into non-overlapping sub-regions and RSSs in the same sub-region are similar. The division process is as follows:

(1) randomly select *K* objects as initial cluster centroids from all SP data objects. Each SP data object is composed of $T \times 4$ RSS elements, where T is the number of acquisition times and 4 represents the number of LEDs in each macro-region.

(2) for all SPs, calculate the Euclidean distance between their data objects and the data object of each cluster centroid in turn. Each SP data object is classified and grouped into the cluster with the smallest Euclidean distance successively. The calculation of the Euclidean distance is as follows:

$$ED(\tilde{S}^{d}, \tilde{\boldsymbol{S}}^{d}) = \sum_{a=0}^{1}\sum_{b=0}^{1}\sqrt{\sum_{t=1}^{T}(\tilde{S}^{d,t}_{(i+a)(j+b)} - \tilde{\boldsymbol{S}}^{d,t}_{(i+a)(j+b)})^{2}} \quad (10)$$

where vector $\tilde{S}^{d}$ represents the RSS observations from a sampling point, vector $\tilde{\boldsymbol{S}}^{d}$ represents the RSS data of the clustering centroid, T is the total number of RS samples collected for each SP. $\tilde{S}^{d,t}_{(i+a)(j+b)}$ and $\tilde{\boldsymbol{S}}^{d,t}_{(i+a)(j+b)}$ represent the *t*-th RSS value of $\tilde{S}^{d}$ and $\tilde{\boldsymbol{S}}^{d}$.

(3) After all SPs are distributed, recalculate the position of the *K* centroids. Delete the clusters that no SP is related to and update the number of valid clusters *K*. Then we calculate the arithmetic mean of all observation values of the SPs assigned to the corresponding cluster as the RSS value of each centroid:

$$\boldsymbol{\mu}^{idc} = \frac{1}{\sum_{\tilde{S}^d \in \widetilde{RS}^{idc}} 1} \cdot \sum_{a=0}^{1} \sum_{b=0}^{1} \sum_{t=1}^{T} \tilde{S}^{d,t}_{(i+a)(j+b)} \quad (11)$$

where *idc* is the identifier of a cluster, $\widetilde{RS}^{idc}$ is the set of normalized observations belonging to SPs assigned to this cluster, and $\boldsymbol{\mu}^{idc}$ is the *idc*-th cluster's centroid, where $1 \leq idc \leq K$.

(4) Repeat (2) and (3) until each cluster converges at its centroid, which is measured by a threshold we preset.

step 3. Training of Radom Forest Classifier

After the SPs are grouped into *K* sub-regions, different classifiers are trained using different training sets derived from $\widetilde{RS}$. For each cluster, a classifier CL_{idc} is trained using $\widetilde{RS}_{idc}$, a subset of $\widetilde{RS}$ only consisting of the observation values from SPs assigned to cluster *idc*. By doing this, each sub-classifier CL_{idc} only needs to handle a specific and smaller data subset, thus greatly simplifying the classification problem. For the classifiers suitable for the algorithm implementation, the Random Forest is selected in this paper due to its accuracy and efficiency, which are critical for indoor real-time positioning.

The RF algorithm grows a collection of decision trees and uses them for classifying a SP into one of the classes. Given a data set on *N* samples for training, $Z = \{(\tilde{S}^1, C^1), (\tilde{S}^2, C^2), \ldots, (\tilde{S}^d, C^d), \ldots, (\tilde{S}^N, C^N)\}$, where $\tilde{S}^d$, d=1,2,...,N, N is the number of samples in the training set. Let P be the number of variables in the classifier and p be the input parameter denoting the number of input variables to be used to determine the decision at a node of the tree. Usually $p \ll P$. And RF can be implemented as follows:

(1) Repeat for ε=1, 2, . . . , ntree:

(a) Pick N samples randomly from the training set with replacement and get a "bootstrap set", Z^*= $\{(\tilde{S}^{*1}, C^{*1}), (\tilde{S}^{*2}, C^{*2}), \ldots, (\tilde{S}^{*N}, C^{*N})\}$.

(b) In the bootstrap set, about two-thirds of the original training samples are used to grow a classification tree. About one-third of the samples are left and used to obtain unbiased estimates of correct classification rates and variable importance.

(c) At each node, randomly choose p variables on which to base the decision at that node. Calculate the best split based on these p variables in the training set.

(d) Each tree is fully grown and not pruned. That is, each tree is constructed using the bootstrap samples of the training data and random feature selection.

(2) After the number ntree of iterations is achieved (i.e., ntree trees are grown), predictions for test data can be carried out. To classify a new object, the sample is given as input at each of decision trees in the forest; each tree gives a classification and the final class is chosen on the basis of the majority vote rule. On the basis of the distribution of votes among the different classes, a confidence is also computed for each class. Specifically, given a class η, the related confidence c_η corresponds to the percentage of votes obtained through a series of decision trees composing the classifier.

By this way, the input parameters of the K-Means are set, and the input parameters of the RF algorithm in each sub-region are adjusted to obtain optimal location, which together with the K value of K-Means and the initial cluster centroid point will be used for the online positioning stage.

2.3.2 Online Positioning: Efficient Matching of Fingerprint Data Based on Fusion of K-Means and Random Forest Algorithm

During the positioning stage, a new observation S^{new} is inputted into the system in order to predict the actual location of the observation point. The localization process can also be divided into three steps:

- Data Normalization
- Sub-region Classification Based on K-Means
- Reclassification Based on Random Forest

step 1. Data Normalization

According to the maximum and minimum RSS values of each LED obtained in the training phase, the new observation S^{new} is normalized as described in step 1, Section 2.3.1, thus obtaining $\tilde{S}^{new}$. Since some feature values could be out of the maximum and minimum bounds, a clipping operation is performed to preserve values in the range [0; 1]:

$$\tilde{S}^{new}_{(i+a)(j+b)} = \begin{cases} 0, & v < 0 \\ 1, & v > 1 \\ v, & o.w. \end{cases} \tag{12}$$

where

$$v = \frac{S^{new}_{(i+a)(j+b)} - m_{ab}}{M_{ab} - m_{ab}} \tag{13}$$

step 2. Sub-region Classification Based on K-Means

From Section 2.3.1, we know that in offline stage, each macro-region has been partitioned into a number of non-overlapping sub-regions. In this step, the K-Means classifier is used to cluster the normalized new observation $\tilde{S}^{d}$, distinguishing among the different sub-regions and determining which sub-region the observation resides. The Specific determining process is to calculate the Euclidean distance from $\tilde{S}^{d}$ to the cluster centroid of each sub-region, select the minimum value of

the Euclidean distance, and group the observation value into this sub-region. The process above is recorded as $KC_{\tilde{S}^{new}}$:

$$KC_{\tilde{S}^{new}} = \min(ED(\tilde{S}^{new}, \boldsymbol{\mu}^{idc})) \quad (14)$$

step 3. Reclassification Based on Random Forest

In this step, the classifier, corresponding to the selected sub-region in Step 2, is used to predict the location point where the signal is observed. When a new sample to be classified is input into each tree in the forest, each tree will give a classification result. The final classification result is determined by the majority voting rule. According to the voting distribution of different classes, the confidence level of each class is calculated. Specifically, for class *idp*, its confidence $c_{\boldsymbol{idp}}$ denotes the percentage of votes cast by a series of decision trees in the classifier.

Suppose that the K-Means classifier has grouped the new observation $\tilde{S}^{new}$ into sub-region *idc*. Then the well-trained RF model CL_{idc} will be utilized to conduct a reclassification on $\tilde{S}^{new}$. And the reclassification result can be expressed by a set of confidence values as follows:

$$Conf_{idc} = \{c_{\boldsymbol{idp}}, idp \in C_{\boldsymbol{idc}}\} \quad (15)$$

where $C_{\boldsymbol{idc}}$ is the set of all identifiers of SPs assigned to the sub-region *idc*, containing all possible location points that are predicted, and $c_{\boldsymbol{idp}}$ represents the likelihood that the observation point is located at the point *idp*. Here we choose the location point with the highest confidence as C^{new}, the estimated location for the observation value $\tilde{S}^{new}$.

3 Simulation and Analysis

3.1 Indoor Three-dimensional Fusion Positioning Simulation Model Using Fingerprinting

Simulation is launched to evaluate the stability and accuracy of our mentioned system. In this section, an indoor VLC-based positioning system with a 2 m × 2 m × 3 m environment is established. As described in Fig. 3, the fingerprinting-based VLP kernel includes four LEDs located on the ceiling. We generated the 3-D localization fingerprint database in the mentioned kernel, where the sampling points are randomly and evenly distributed. The main parameters of the proposed indoor three-dimensional fusion positioning simulation model using K-Means and Random Forest can be seen in Table 1. In the offline stage, the fusion positioning model needs to be trained for position estimation. Since a great deal of fingerprint data can be obtained easily through simulation, we chose 10000, 20000, 30000, 40000, and 50000 as training data sizes respectively to compare their positioning performances. In our simulation, minimum leaf node size is set to 50 and maximum tree depth is set to 20.

The larger the fingerprint database is, the higher the positioning accuracy will be. But the enlargement of fingerprint database size will lead to the aggravation of computer's computational load. As shown in Fig. 6, when the number of sampling points of fingerprint database increase from 10000 to 50000, the training time increases rapidly while the average positioning error does not drop significantly. That means, an excessive fingerprint database will only bring about time-consuming operation without obvious improvement in positioning accuracy. And if we fix the fingerprint database size to 10000, the number of decision trees' effect on positioning performance can be shown in Fig. 7. We also have to strike a balance between computing time and positioning accuracy. Therefore, in the following simulations, we set the fingerprint database density to 10000/12 m^3 and the number of decision trees to 130.

Table1 Simulation parameters

Parameter	Value

Size of the fingerprint-based VLP kernel (length×width×height) /m	2 m×2 m×3 m
Power of each LED /W	9W
Position of the four LEDs (X,Y,Z) /m	$\mathrm{LED}_{11}(0,0,3)$ $\mathrm{LED}_{12}(0,2,3)$ $\mathrm{LED}_{21}(2,0,3)$
The number of sampling dots of fingerprint database	10000/20000/30000/40000/50000
Height of the receiver /m	0.3 to 2.4 (resolution:0.3)
Plane range of the receiver /m	(0.3, 0.3) to (1.8, 1.8) (resolution:0.3)
The FOV of the transmitters /deg	60
The FOV of the receiver /deg	70
The diameter of the PD/mm	14
The photoelectric transformation efficiency/A·W^{-1}	0.35
The gain of optical filter $[T(\Psi_{ij}^{k})]$	1.0
The gain of optical concentrator $[G(\Psi_{ij}^{k})]$	1.0
Number of decision trees	130
Minimum leaf node size	50
Maximum tree depth	20

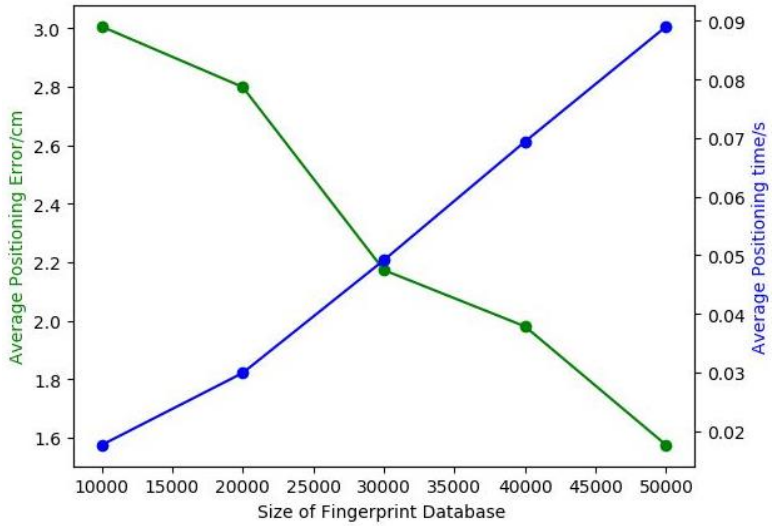

Fig. 6. The positioning error and time with different size of fingerprint database.

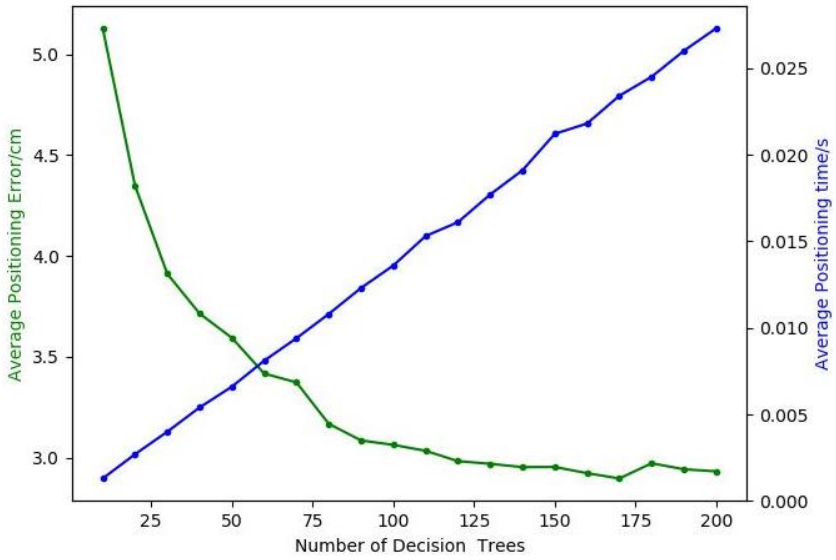

Fig. 7. The positioning error and time with different number of decision trees.

3.2 Results and Analysis

3.2.1 Multi-Point Testing

The 3-D positioning simulation results in the fingerprinting-based VLP kernel are discussed in this section. The height resolution of the test positions is 0.3 m from 0.3 m to 2.4 m and 288 positions are included totally. Results are shown in Fig. 8, where green dots represent the estimated positions and red dots represent the exact positions.

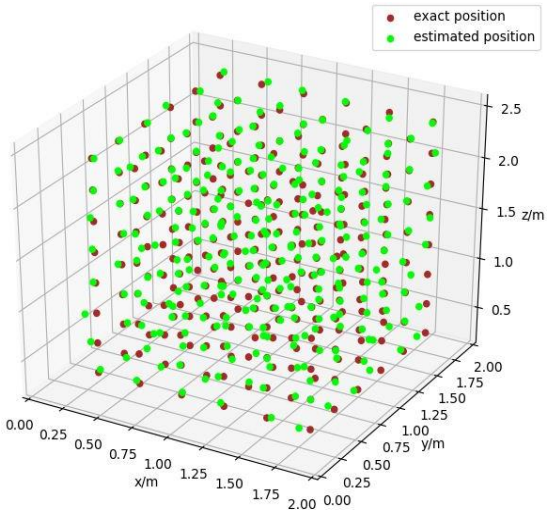

Fig. 8. Three-dimensional positioning effect with fusion of KM and RF.

As can be seen from the curves in Fig. 9, 90% of the 3-D positioning errors of fusion of KM and RF algorithm is under 5.8 cm and the average error is 2.9642 cm. As shown by histograms in Fig.10, the maximum 3-D error of 288 test points is 10.39 cm and the minimum 3-D error is 0.21 cm. And most of the 3-D positioning errors are below 4 cm. Besides, most of the vertical positioning errors are below 1.00 cm.

The whole simulation result of 3-D visible light fingerprinting positioning using fusion of KM and RF algorithm is layered and displayed in Fig. 11, and the average errors of the test positions are tagged in the six figures severally. The positioning results of simulation achieve a minor error of less than 1.05 cm at more than 30 test points, which shows that the fusion of KM and RF algorithm for VLP using fingerprinting works accurately on the whole.

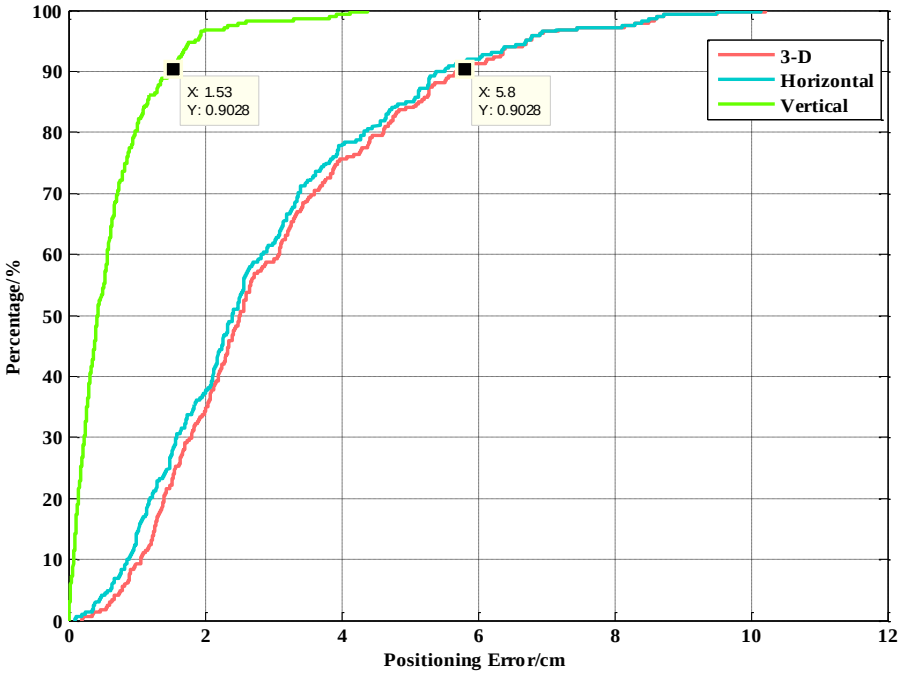

Fig. 9. The 3-D, vertical, and horizontal CDF curves of positioning error using fusion of KM and RF.

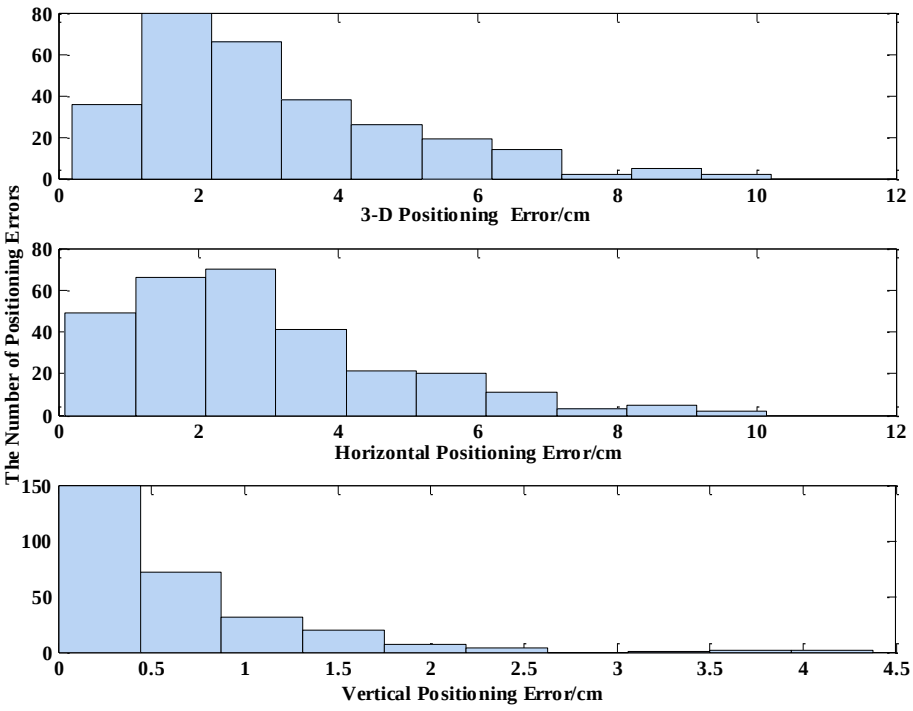

Fig.10. Histogram of positioning errors in three dimensions.

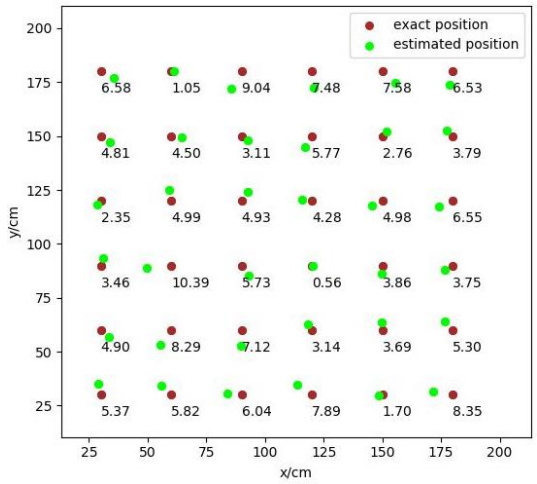
exact position
estimated position
6.58 1.05 9.04 7.48 7.58 6.53
4.81 4.50 3.11 5.77 2.76 3.79
2.35 4.99 4.93 4.28 4.98 6.55
3.46 10.39 5.73 0.56 3.86 3.75
4.90 8.29 7.12 3.14 3.69 5.30
5.37 5.82 6.04 7.89 1.70 8.35
y/cm
x/cm

(a)

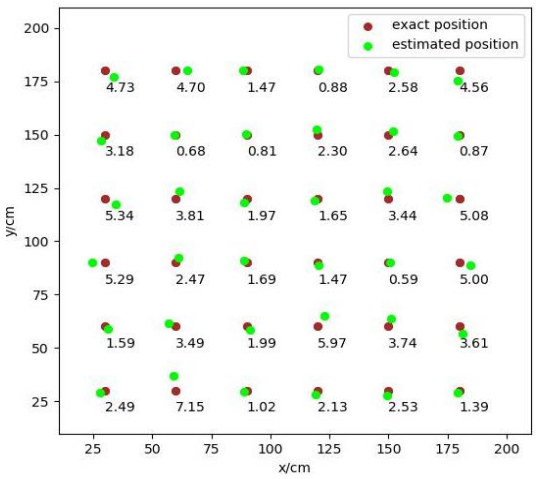
exact position
estimated position
4.73 4.70 1.47 0.88 2.58 4.56
3.18 0.68 0.81 2.30 2.64 0.87
5.34 3.81 1.97 1.65 3.44 5.08
5.29 2.47 1.69 1.47 0.59 5.00
1.59 3.49 1.99 5.97 3.74 3.61
2.49 7.15 1.02 2.13 2.53 1.39
y/cm
x/cm

(b)

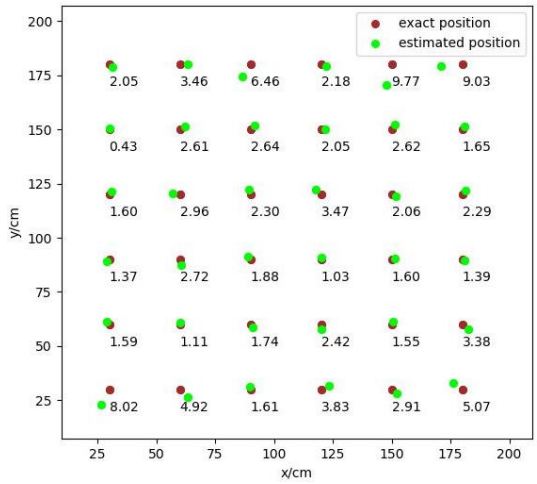
exact position
estimated position
2.05 3.46 6.46 2.18 9.77 9.03
0.43 2.61 2.64 2.05 2.62 1.65
1.60 2.96 2.30 3.47 2.06 2.29
1.37 2.72 1.88 1.03 1.60 1.39
1.59 1.11 1.74 2.42 1.55 3.38
8.02 4.92 1.61 3.83 2.91 5.07
y/cm
x/cm

(c)

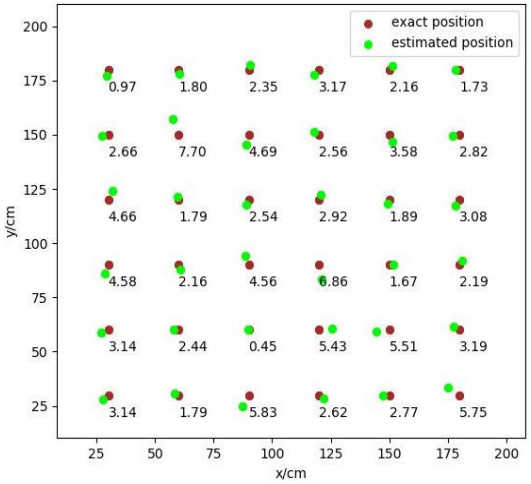
exact position
estimated position
0.97 1.80 2.35 3.17 2.16 1.73
2.66 7.70 4.69 2.56 3.58 2.82
4.66 1.79 2.54 2.92 1.89 3.08
4.58 2.16 4.56 6.86 1.67 2.19
3.14 2.44 0.45 5.43 5.51 3.19
3.14 1.79 5.83 2.62 2.77 5.75
y/cm
x/cm

(d)

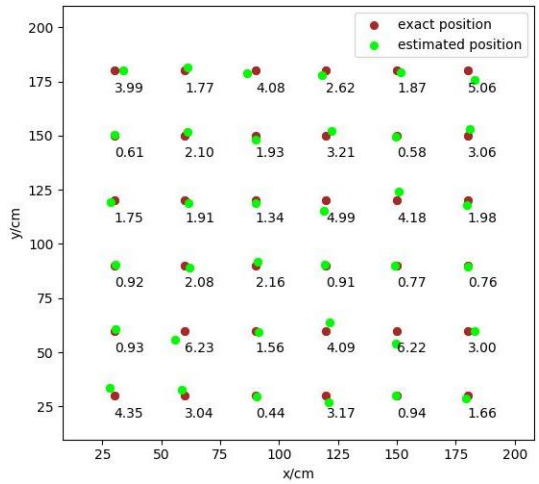
exact position
estimated position
3.99 1.77 4.08 2.62 1.87 5.06
0.61 2.10 1.93 3.21 0.58 3.06
1.75 1.91 1.34 4.99 4.18 1.98
0.92 2.08 2.16 0.91 0.77 0.76
0.93 6.23 1.56 4.09 6.22 3.00
4.35 3.04 0.44 3.17 0.94 1.66
y/cm
x/cm

(e)

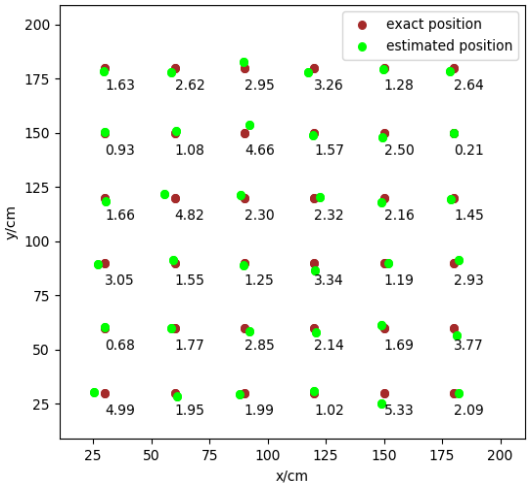
exact position
estimated position
1.63 2.62 2.95 3.26 1.28 2.64
0.93 1.08 4.66 1.57 2.50 0.21
1.66 4.82 2.30 2.32 2.16 1.45
3.05 1.55 1.25 3.34 1.19 2.93
0.68 1.77 2.85 2.14 1.69 3.77
4.99 1.95 1.99 1.02 5.33 2.09
y/cm
x/cm

(f)

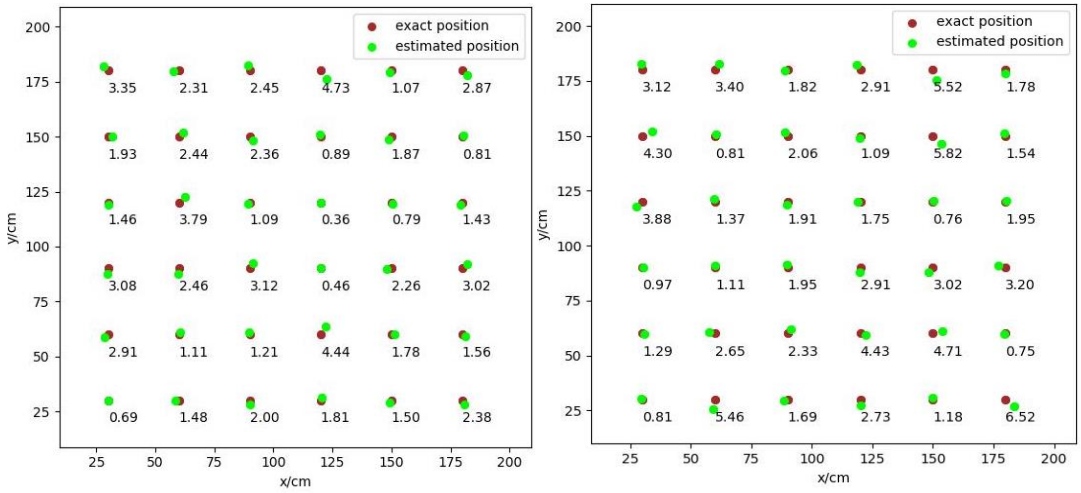

(g) (h)

Fig. 11. Estimated positions and 3-D positioning errors of the simulation with different heights: (a)~(h) represent the 3-D positioning results of 0.3 m, 0.6 m, 0.9 m, 1.2 m, 1.5 m, 1.8 m, 2.1m, 2.4 m high position points, respectively.

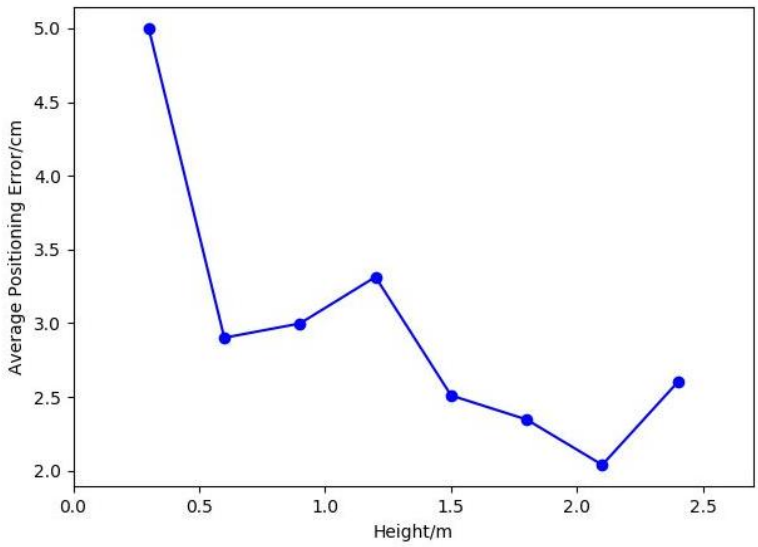

Fig. 12. Average positioning error with different heights.

Fig. 12 visually presents that the average positioning error decreases with the height in general, especially when the height is less than 0.6 m. And the average positioning error at the minimum height of 0.3 m is smaller than 5.50 cm.

3.2.2 Positioning in Motion Scene

To test the real-time performance of proposed algorithm, another simulation experiment of motion positioning is carried out. In this simulation, two random paths are given by assuming a moving target in the positioning unit at a speed of around 1m/s. There are 758 samples in Fig.13 (a), and 361 samples in Fig.13 (b). In this figure, the red tracks are the random paths and the green points are the estimated locations that track the path. The positioning results in Fig.13 show that the fusion of KM and RF algorithm performs well in motion scene with an average 3-D positioning error of 3.12 cm in (a) and 2.50 cm in (b).

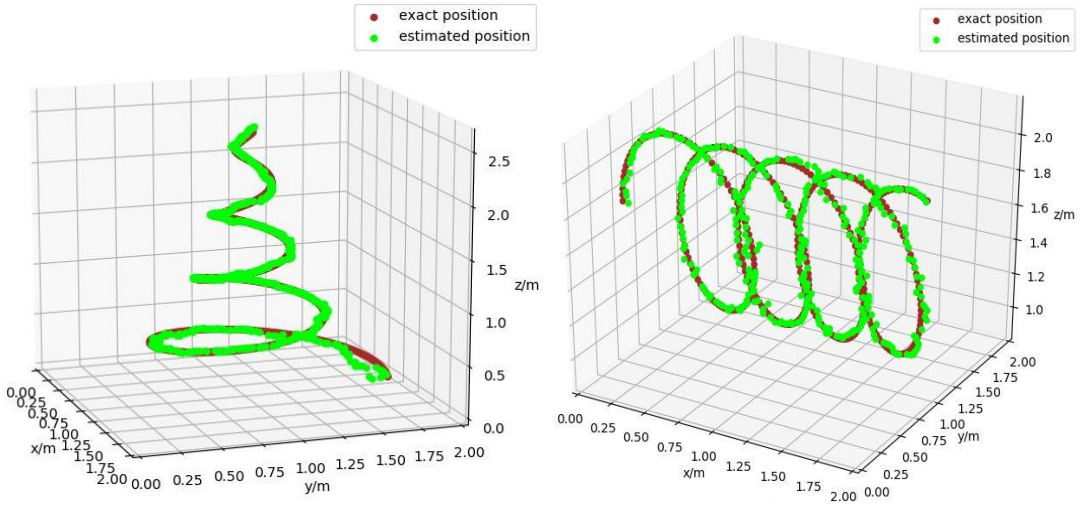

(a) (b)

Fig. 13. 3-D positioning results in motion positioning.

Table 2 Experiment Parameters

Parameter	Reference
Indoor space unit size (L × W × H)/m^3	0.9m × 1.1m × 1.7m
Positions of four LEDs (x, y, z)/m	LED1 (0, 0, 1.7) LED2 (0.9, 0, 1.7) LED3 (0.9, 1.1, 1.7) LED4 (0, 1.1, 1.7)
Height of the receiver /m	0.25, 0.5, 0.75, 1.0, 1.25, 1.5
X,Y Plane range of the receiver /m	X: 0.1 to 0.7(resolution: 0.2) Y: 0.1 to 1.1(resolution: 0.2)

The effective area of PD /cm^2	1.0
Frequency of the light signals/Hz	400,800,1600,3200

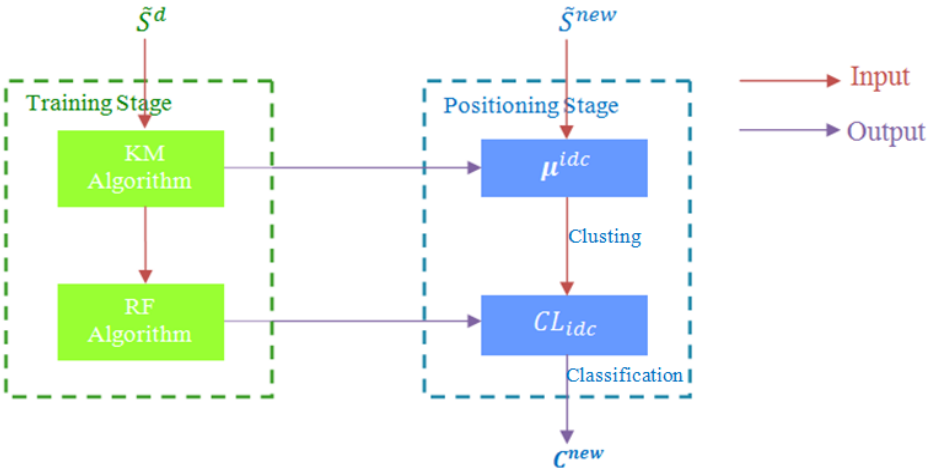

Fig. 14. The system structure of the fusion positioning system.

4 Experiment and Results

4.1 Experiment Setup

Establishment of the fingerprinting-based VLP kernel platform: The experiment shown in Fig. 17 is established to verify the practicality and feasibility of the system and validate our theoretical analysis. It imitates real VLC scenes, which satisfies the needs of positioning and lighting simultaneously. Four LEDs as signal generator are installed in a cube frame with a size of 0.9 m × 1.1 m × 1.7 m, which serves as the fingerprinting-based VLP kernel for large-scale LED scenes. The transmitting part consists of a computer (Laptop1), a STM32F407, a LED driving circuit and LEDs. The receiving part is composed of a photodiode circuit, a STM32F407 and a computer (Laptop2) that communicates with STM32F407 via USB serial port. The parameters of the experiment are shown in Table 2. The Structure of the proposed VLC-based fusion positioning system using fingerprinting integrating KM and RF is shown in Fig.14, and the pseudo codes for the proposed algorithm can be seen in Fig.15 and Fig.16.

Hardware Design: Laptop1 at transmitting end indirectly controls the information and the position ID of LEDs by serial communication with STM32F407ZG. STM32F407ZG receives the data from Laptop1 and sends data to the LED driving circuit (DD311). The driving circuit applies the resulting waveform to the LEDs and the PD at receiving terminal detects the light signals, the frequencies of which are set 400 Hz, 800 Hz, 1600 Hz and 3200 Hz respectively. After light signals are detected and transmitted to a two-stage amplifier circuit (made up of OPA657), STM32F407ZGT6 acquires the ADC measurement and obtains the RSS value. Meanwhile, the amplified signals pass through a voltage comparator circuit (made up of LM393), then demodulated and decoded by STM32F407ZGT6 to obtain the LED's position ID. Next, the data of received signals are delivered to Laptop2, where we use Fusion of KM and RF algorithm to calculate the receiver's position. The circuit diagrams and circuit boards of transmitter and receiving terminal are shown in Figs.18-21 respectively.

Algorithm 1 K-Means Clustering

Training Stage:
Input: K, $\tilde{S}^d$, $\tilde{\boldsymbol{S}}^{idc}$
Output: $\boldsymbol{\mu}^{idc}$
1: Create K points as the initial centroid by random selection
2: **for** $\tilde{S}^d$ such that $1 \le d \le D$ do
3: **for** $\tilde{\boldsymbol{S}}^{idc}$ such that $1 \le idc \le K$ do
4: Calculate Euclidean distance between $\tilde{S}^d$ and $\tilde{\boldsymbol{S}}^{idc}$
5: **end for**
6: Group $\tilde{S}^d$ into cluster with $\min(ED(\tilde{S}^d, \tilde{\boldsymbol{S}}^{idc}))$
7: **end for**
8: **for** $1 \le idc \le K$ do
9: $\boldsymbol{\mu}^{idc} \leftarrow$ arithmetic mean of $\tilde{S}^d$ of cluster idc
10: **end for**
Positioning Stage:
Input: $\tilde{S}^{new}$, $\boldsymbol{\mu}^{idc}$
Output: $KC_{\tilde{S}^{new}}$
1: **for** $1 \le idc \le K$ do
2: Group $\tilde{S}^{new}$ into cluster with $\min(ED(\tilde{S}^d, \boldsymbol{\mu}^{idc}))$
3: **end for**

Fig. 15. The pseudo code of KM algorithm for VLP using fingerprint.

Algorithm 2 Random Forest Classification

Training Stage:
Input: $\widehat{RS}_{idc}$, Z, P, p
Output: CL_{idc}
1: **for** $1 \le \varepsilon \le ntree$ do
2: Draw a bootstrap sample Z^* of size N from the training data
3: Grow a random-forest tree T_ε to the bootstrapped data
4: **do**
5: **for** each terminal node for the tree
6: Select m variables at random from p variables
7: Pick the best variable/spilt-point from the m
8: Spilt the node into two daughter nodes
9: **end for**
10: **while** minimum leaf node size and maximum tree depth are not reached
11: **end for**
12: $CL_{idc} \leftarrow$ ensemble of T_ε
Positioning Stage:
Input: $\tilde{S}^{new}$, CL_{idc}
Output: C^{new}
1: **for** $1 \le idc \le K$ do
2: Choose the idp with max($Conf_{idc}$)
3: **end for**

Fig. 16. The pseudo code of RF algorithm for VLP using fingerprint.

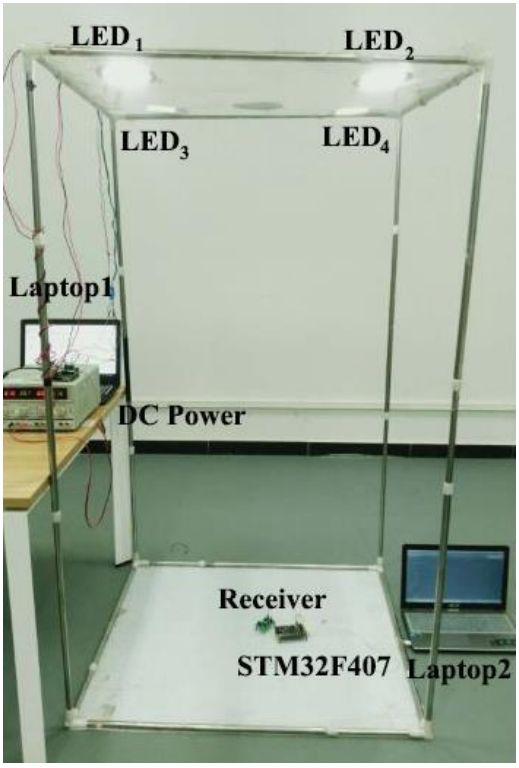

Fig. 17. Experimental platform of VLC system based on DBOM-based ACO.

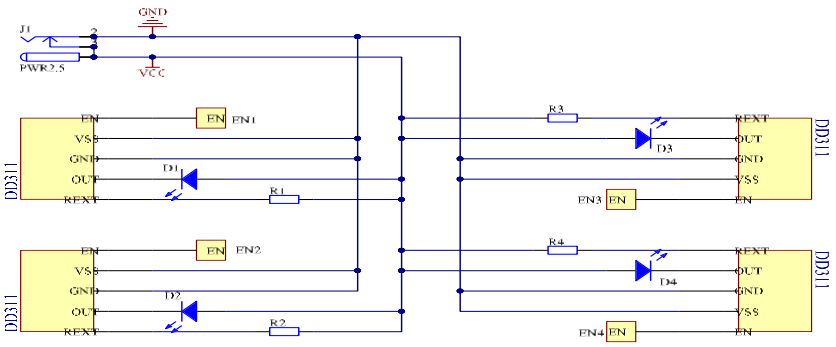

Fig. 18. The circuit diagrams of transmitting terminal.

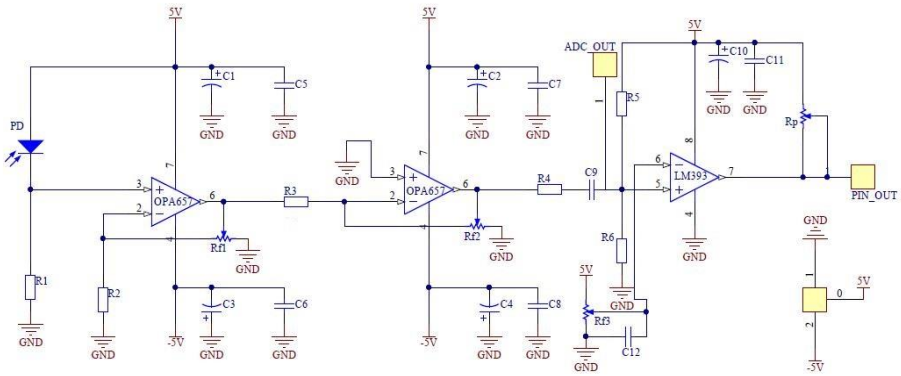

Fig. 19. The circuit diagrams of receiver terminal.

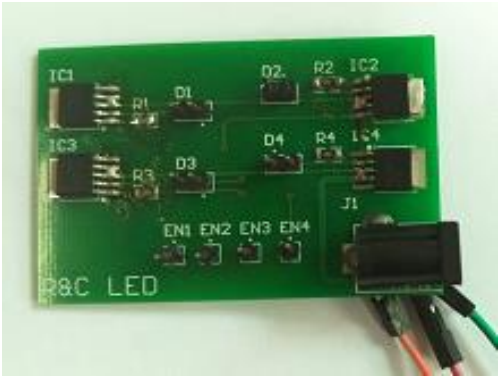

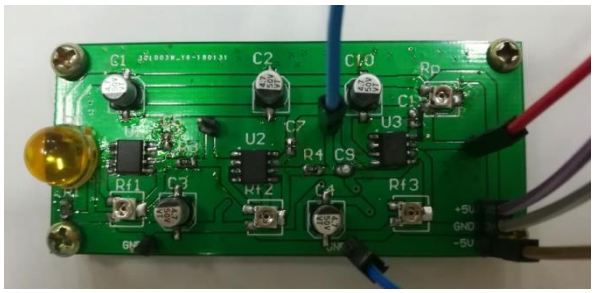

Fig. 20. The circuit board of transmitting terminal. Fig. 21. The circuit board of receiver terminal.

4.2 Results and Analyze

In the experiment, we collected 1200 sets of data to set up a fingerprint database and trained it using the proposed algorithm. There are 16 test points evenly distributed at the height of 0.3 m, 0.6 m, 0.9 m and 1.2 m respectively. So 144 positions are tested in the experiment totally. At each test position, the proposed fusion of KM and RF algorithm for VLP using fingerprint is applied to calculate the estimated position. The position results are shown in Figs. 24-26 and the 3-D average positioning errors of the test positions are written in the figures strictly as the experiment results show. Experiment results suggest that the average 3-D error is 4.45 cm and the maximum error is 10.67 cm. Over 90% of the errors are within 7.58 cm. And average time spent for positioning each test point is 0.002596 s. The CDF curves are shown in Fig. 25, and the histograms of 3-D error, horizontal error and vertical error of the experiment are shown in Fig. 26. The results indicate that the proposed positioning system based on VLC and fingerprinting using fusion of KM and RF algorithm performs well in accuracy and real-time ability.

The errors mainly result from the following reasons. Firstly, data sampling in real scene is difficult, so it is impractical for the data size to reach 10,000 or even 100,000. Therefore, the reduction of the fingerprint database size directly affects positioning accuracy. Secondly, the light intensity of LEDs varies slightly with time due to the aging of LEDs, poor heat dissipation, instability of driving current or other reasons, causing that the RSS value received at the same location point changes with time. Finally, measurement error also causes accidental error. Nevertheless, the experiment results still prove that our proposed system attains the accuracy requirement of cm-level indoor positioning.

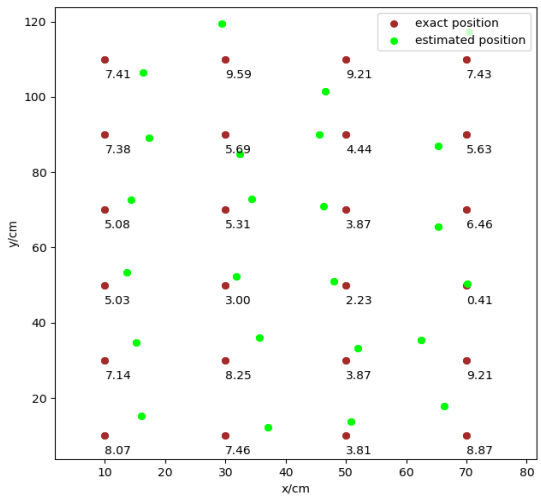
exact position
estimated position
7.41 9.59 9.21 7.43
7.38 5.69 4.44 5.63
5.08 5.31 3.87 6.46
5.03 3.00 2.23 0.41
7.14 8.25 3.87 9.21
8.07 7.46 3.81 8.87
y/cm
x/cm

(a)

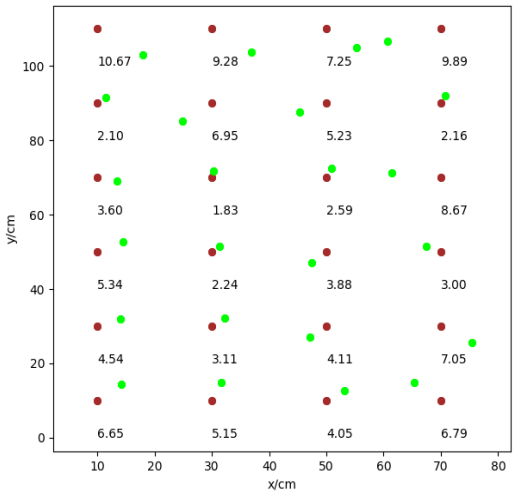
10.67 9.28 7.25 9.89
2.10 6.95 5.23 2.16
3.60 1.83 2.59 8.67
5.34 2.24 3.88 3.00
4.54 3.11 4.11 7.05
6.65 5.15 4.05 6.79
y/cm
x/cm

(b)

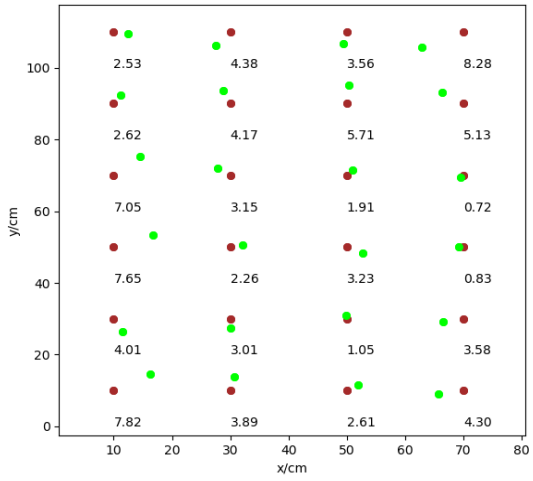
2.53 4.38 3.56 8.28
2.62 4.17 5.71 5.13
7.05 3.15 1.91 0.72
7.65 2.26 3.23 0.83
4.01 3.01 1.05 3.58
7.82 3.89 2.61 4.30
y/cm
x/cm

(c)

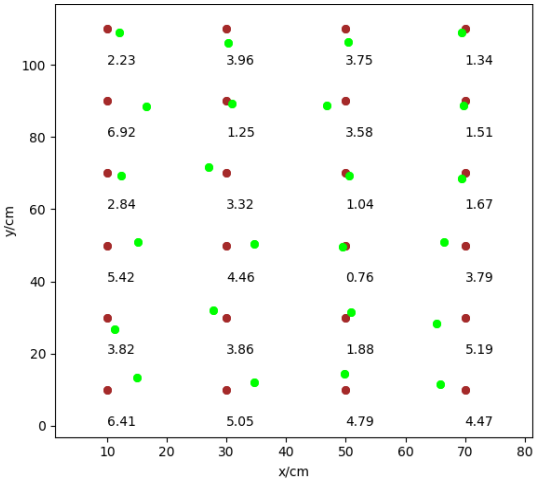
2.23 3.96 3.75 1.34
6.92 1.25 3.58 1.51
2.84 3.32 1.04 1.67
5.42 4.46 0.76 3.79
3.82 3.86 1.88 5.19
6.41 5.05 4.79 4.47
y/cm
x/cm

(d)

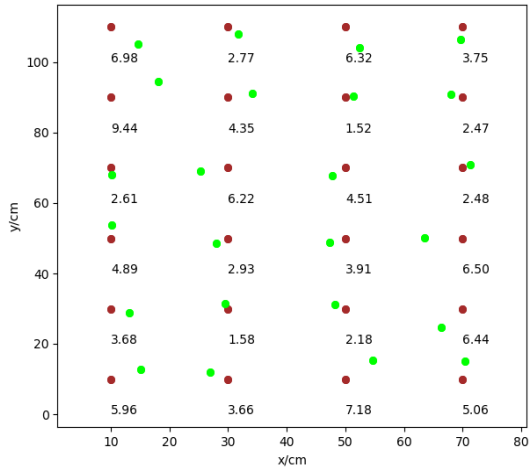
6.98 2.77 6.32 3.75
9.44 4.35 1.52 2.47
2.61 6.22 4.51 2.48
4.89 2.93 3.91 6.50
3.68 1.58 2.18 6.44
5.96 3.66 7.18 5.06
y/cm
x/cm

(e)

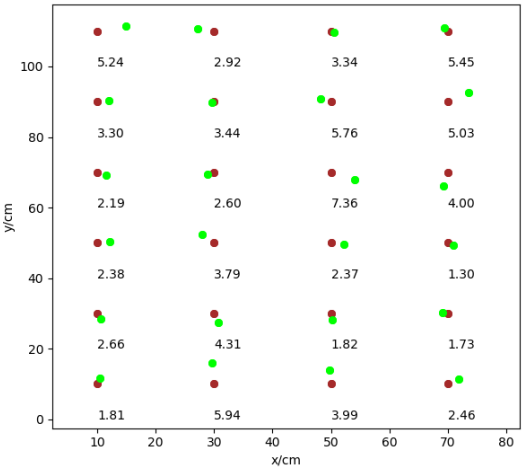
5.24 2.92 3.34 5.45
3.30 3.44 5.76 5.03
2.19 2.60 7.36 4.00
2.38 3.79 2.37 1.30
2.66 4.31 1.82 1.73
1.81 5.94 3.99 2.46
y/cm
x/cm

(f)

Fig. 22. Estimated positions and 3-D positioning errors of the experiment. with different heights: (a)~(f) represent the 3-D positioning results of 0.25 m, 0.5 m, 0.75 m, 1.0 m, 1.25 m, 1.5 m high position points, respectively.

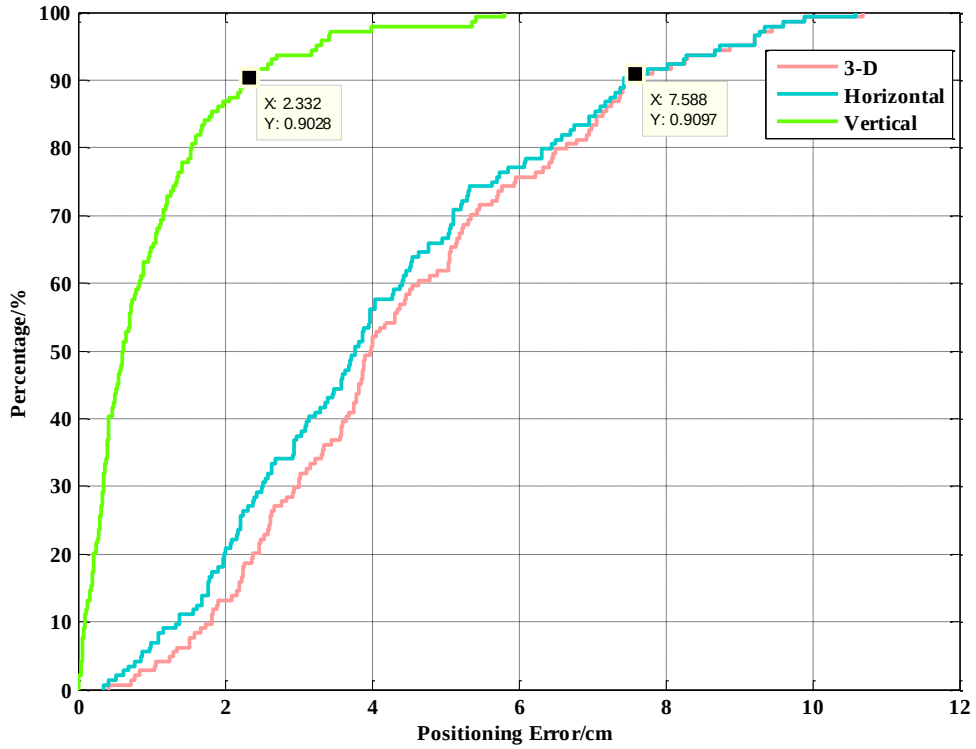

Fig. 23. The 3-D, vertical and horizontal CDF curves for experiment.

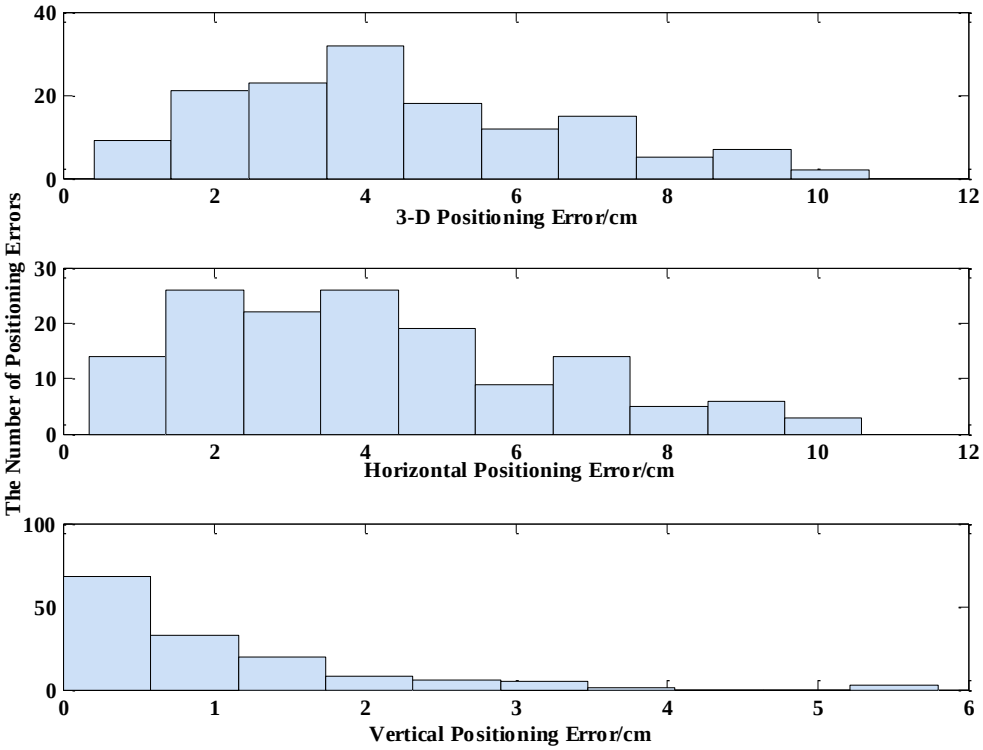

Fig. 24. Histogram of positioning errors for experiment.

5 Conclusion

In order to adapt VLP algorithm to the complex indoor location environment with large-scale LEDs, this paper puts forwards an indoor three-dimensional visible light fingerprint positioning system based on fusion of K-Means (KM) and Random Forest (RF) algorithm. We partition the large indoor location environment into a good number of macro-regions, which can be unified and summarized as a fingerprinting-based VLP kernel. In the positioning kernel, the fusion of KM and RF algorithm is utilized to realize 3-D VLC-based positioning. Our proposed algorithm includes offline training stage and online positioning stage. In training stage, Firstly, K-Means algorithm divides the located macro-region into several non-overlapping sub-regions through clustering fingerprint data. Secondly, in each sub-region, RF classifier is trained using fingerprints grouped into the corresponding sub-region. In positioning stage, first the KM classifier is used to cluster the observed RSS value from the test point to determine which sub-region it belongs to. Next, the trained RF classifier of the object sub-region carries out a second classifications to the observed value and utilize the output results of decision trees to generate the final position estimate. The experimental results show the average 3-D location error of the proposed system is 4.45 cm. It verifies that the proposed 3-D fingerprinting-based positioning system can achieve cm-level indoor positioning with strong interference immunity and great real-time ability, which makes it a promising candidate for future large-scale indoor positioning applications.

6 Reference

[1] X. S. Guo, L. Chu, B. Li, B. Xu, Q. Wan, and Y. Shen, “A robust vector matching localization approach based on multiple channels SSD fingerprinting of zigbee networks,” Prog. Electromagn. Res., vol. 144, no. 1, pp. 133–140, 2014.

[2] X. Guo, L. Chu, and X. Sun, “Accurate localization of multiple sources using semidefinite programming based on incomplete range matrix,” IEEE Sens. J., vol. 16, no. 13, pp. 5319–5324, Jul. 2016.

[3] X. Guo and N. Ansari, “Localization by fusing a group of fingerprints via multiple antennas in indoor environment,” IEEE Trans. Veh. Technol., vol. PP, no. 99, pp. 1–1, Jul. 2017.

[4] G. Wang, S. Cai, Y. Li, and N. Ansari, “A bias-reduced nonlinear WLS method for TDOA/FDOA-based source localization,” IEEE Trans. Veh. Technol., vol. 65, no. 10, pp. 8603–8615, Oct. 2016.

[5] S. Shao, A. Khreishah, and H. Elgala, “Pixelated VLC-backscattering for self-charging indoor IoT devices,” IEEE Photon. Technol. Lett., vol. 29, no. 2, pp. 177–180, Nov. 2017.

[6] J. K. Park, T. G. Woo, M. Kim, and J. T. Kim, “Hadamard matrix design for a low-cost indoor positioning system in visible light communication,” IEEE Photon. J., vol. 9, no. 2, Apr. 2017, Art. no. 7801710.

[7] S. Kuntze, A. J. Zilkie, L. Pavel, and J. S. Aitchison, “Nonlinear state-space model of semiconductor optical amplifiers with gain compression for system design and analysis,” J. Lightw. Technol., vol. 26, no. 14, pp. 2274–2281, Jul. 2008.

[8] Do Trong-Hop and Yoo Myungsik, “An in-depth survey of visible light communication based positioning systems [J],” Sensors,vol. 16, no. 5, 2016, Art. no. E678.

[9]Yang Se-Hoon, Kim Hyun-Seung, Son Yong-Hwan, and Han Sang-Kook, “Three-dimensional visible light indoor localization using AOA and RSS with multiple optical receivers [J],” J. Lightwave Technol., vol. 32, no. 14, pp. 2480–2485, Jul. 15, 2014.

[10]Weipeng Guan, Yuxiang Wu, Shangsheng Wen, Hao Chen, Yingcong Chen, Z. Zhang,“A novel three-dimensional indoor positioning algorithm design based on visible light communication [J],” Optics Communications, vol. 392, pp. 282-293, June 1, 2017.

[11]Weipeng Guan, Yuxiang Wu, Shangsheng Wen, Yang Chen, Hao Chen, Zhaoze Zhang, Yingcong Chen. “High precision three-dimensional iterative indoor localization algorithm using code division multiple access modulation based on visible light communication [J],” Optical Engineering, vol. 55, no. 10, October 1, 2016.

[12] Weipeng Guan, Yuxiang Wu, Shangsheng Wen, Yirong Chen, Hao Chen. “Indoor positioning technology of visible light communication based on CDMA modulation [J],” Acta Optica Sinica, vol. 36, no. 11, November 10, 2016.

[13] Hao Chen, Weipeng Guan, Simin Li, Yuxiang Wu, “Indoor High Precision Three-Dimensional Positioning System Based On Visible Light Communication Using Modified Genetic Algorithm,” Opt. Commun., vol. 413, Dec. 15, 2017.

[14] Huanhuan Zheng, Zhaowen Xu, Changyuan Yua, and Gurusamy Mohan, “A 3-D high accuracy positioning system based on visible light communication with novel positioning algorithm,” [J]. Opt. Commun., 2017, Vol.396, pp.160-168.

[15] Ye Cai, Weipeng Guan, Yuxiang Wu, Canyu Xie, Yirong Chen, and Liangtao Fang, “Indoor High Precision Three-Dimensional Positioning System Based On Visible Light Communication Using Particle Swarm Optimization,” IEEE Photon. J., vol. 9, no. 6, Dec, 2017.

[16] Yuxiang Wu, Xiaowei Liu, Weipeng Guan, Bangdong Chen, Xin Chen and Canyu Xie," High-Speed 3D Indoor Location System based on Visible Light Communication using Differential Evolution Algorithm [J]," Optics Communications, pp.177-189,2018, Vol.424.

[17] K. Kaemarungsi, P. Krishnamurthy, "Modeling of indoor positioning systems based on location fingerprinting," INFOCOM 2004. Twenty-third AnnualJoint Conference of the IEEE Computer and Communications Societies, pp.1012-1022, 2004, DOI: 10.1109/INFCOM.2004.1356988.

[18] Chin-Wei Hsu, Siming Liu, Feng Lu, Chi-Wai Chow, Chien-Hung Yeh and Gee-Kung Chang, "Accurate Indoor Visible Light Positioning System utilizing Machine Learning Technique with Height Tolerance," OFC 2018, M2K.2.; and DOI: 10.1109/JPHOT.2016.2590945.

[19] Ming Xu, Weiwei Xia, Ziyan Jia, Yaping Zhu, Lianfeng Shen, "A VLC-Based 3-D Indoor Positioning System Using Fingerprinting and K-Nearest Neighbor," Vehicular Technology Conference (VTC Spring), pp. 1-5, Nov. 2017, DOI: 10.1109/VTCSpring.2017.8108345.

[20] Xiansheng Guo, Sihua Shao, Ansari and Nirwan, " Indoor Localization Using Visible Light Via Fusion of Multiple Classifiers," IEEE Photonics Journal, Vol. 9, No. 6, Dec. 2017.

[21] Xuexia Yang, "Expansion Research on K-means Clustering Algorithm Based on Rough Set," EN, 2012, Vol.4(10), pp.221-227.

[22] A. Criminisi, J. Shotton, D. Robertson, and E. Konukoglu, "Regression forests for efficient anatomy detection and localization in CT studies," in Medical Computer Vision Workshop. New York: Springer, 2010, vol. 6533, Lecture Notes in Computer Science, pp. 106–117.

[23] F. Schroff, A. Criminisi, and A. Zisserman, "Object class segmentation using random forests," in Proc. Brit. Mach. Vis. Conf., 2008, pp. 54.1–54.10.

[24] Y. Hou, S. Xiao, M. Bi, Y. Xue, W. Pan, and W. Hu, “Single LED beacon-based 3-D indoor positioning using off-the-shelf devices [J],” IEEE Photon. J., vol. 8, no. 6, Dec. 2016, Art. no. 6806211.

[25] H. S. Kim, D. R. Kim, S. H. Yang, Y. H. Son, and S. K. Han, “An indoor visible light communication positioning system using a RF carrier allocation technique,” J. Lightw. Technol., vol. 31, no. 1, pp. 134–144, Jan. 2012.

Biographies

Jiajia Jiang is currently studying in South China University of Technology at Information Engineering Department for her B.E. degree. Her research interests are in wireless optical communication technology and visible light positioning technology.

Weipeng Guan obtained his B.E. degree from the Electronic Science and Technology Department (Electronic Materials and Components Department) in South China University of Technology, Guangzhou, China, in 2016. He is now working towards the M.E. degree in the Control Theory and Control Engineering Department at South China University of Technology. His research is currently focused on visible light wireless communication technology and visible light positioning technology..

Zhounan Chen is now studying at South China University of Technology in the Automation Science and Engineering Department for his B.E. degree. His research is currently focused on visible light wireless communication technology.

Yirong Chen is currently studying at South China University of Technology in the Electrical Science and Technology Department for his B.E. degree. His research interests are in wireless optical communication technology and visible light positioning technology.

Tables

Table1 Simulation parameters

Parameter	Value
Size of the fingerprint-based VLP kernel (length×width×height) /m	2 m×2 m×3 m
Power of each LED /W	9W
Position of the four LEDs (X,Y,Z) /m	$\mathrm{LED}_{11}(0,0,3)$ $\mathrm{LED}_{12}(0,2,3)$ $\mathrm{LED}_{21}(2,0,3)$
The number of sampling dots of fingerprint database	10000/20000/30000/40000/50000
Height of the receiver /m	0.3 to 2.4 (resolution:0.3)
Plane range of the receiver /m	(0.3, 0.3) to (1.8, 1.8) (resolution:0.3)
The FOV of the transmitters /deg	60
The FOV of the receiver /deg	70
The diameter of the PD/mm	14
The photoelectric transformation efficiency/A·W^{-1}	0.35
The gain of optical filter $[T(\Psi_{ij}^{k})]$	1.0
The gain of optical concentrator $[G(\Psi_{ij}^{k})]$	1.0
Number of decision trees	130
Minimum leaf node size	50
Maximum tree depth	20

Table 2 Experiment Parameters

Parameter	Reference
Indoor space unit size (L × W × H)/m^3	0.9m × 1.1m × 1.7m
Positions of four LEDs (x, y, z)/m	LED1 (0, 0, 1.7) LED2 (0.9, 0, 1.7) LED3 (0.9, 1.1, 1.7) LED4 (0, 1.1, 1.7)
Height of the receiver /m	0.25, 0.5, 0.75, 1.0, 1.25, 1.5
X,Y Plane range of the receiver /m	X: 0.1 to 0.7(resolution: 0.2) Y: 0.1 to 1.1(resolution: 0.2)
The effective area of PD /cm^2	1.0
Frequency of the light signals/Hz	400,800,1600,3200

605

606

607 **List of figure captions**

608 Fig. 1. Indoor optical wireless positioning system.

609 Fig. 2. Macro partition of area in VLC-based positioning using fingerprint.

610 Fig. 3. The scene graphic of indoor VLC-based positioning using fingerprint.

611 Fig. 4. Training Process.

612 Fig. 5. Positioning Process.

613 Fig. 6. The positioning error and time with different size of fingerprint database.

614 Fig. 7. The positioning error and time with different number of decision trees.

615 Fig. 8. Three-dimensional positioning effect with fusion of KM and RF.

616 Fig. 9. The 3-D, vertical, and horizontal CDF curves of positioning error using fusion of KM and RF.

617 Fig.10. Histogram of positioning errors in three dimensions.

618 Fig. 11. Estimated positions and 3-D positioning errors of the simulation with different heights:
619 (a)~(h) represent the 3-D positioning results of 0.3 m, 0.6 m, 0.9 m, 1.2 m, 1.5 m, 1.8 m, 2.1m, 2.4
620 m high position points, respectively.

621 Fig. 12. Average positioning error with different heights.

622 Fig. 13. 3-D positioning results in motion positioning.

623 Fig. 14. The system structure of the fusion positioning system.

624 Fig. 15. The pseudo code of KM algorithm for VLP using fingerprint.

625 Fig. 16. The pseudo code of RF algorithm for VLP using fingerprint.

626 Fig. 17. Experimental platform of VLC system based on DBOM-based ACO.

627 Fig. 18. The circuit diagrams of transmitting terminal.

628 Fig. 19. The circuit diagrams of receiver terminal.

629 Fig. 20. The circuit board of transmitting terminal.

630 Fig. 21. The circuit board of receiver terminal.

631 Fig. 22. Estimated positions and 3-D positioning errors of the experiment. with different heights:
632 (a)~(f) represent the 3-D positioning results of 0.25 m, 0.5 m, 0.75 m, 1.0 m, 1.25 m, 1.5 m high
633 position points, respectively.

634 Fig. 23. The 3-D, vertical and horizontal CDF curves for experiment.

635 Fig. 24. Histogram of positioning errors for experiment.

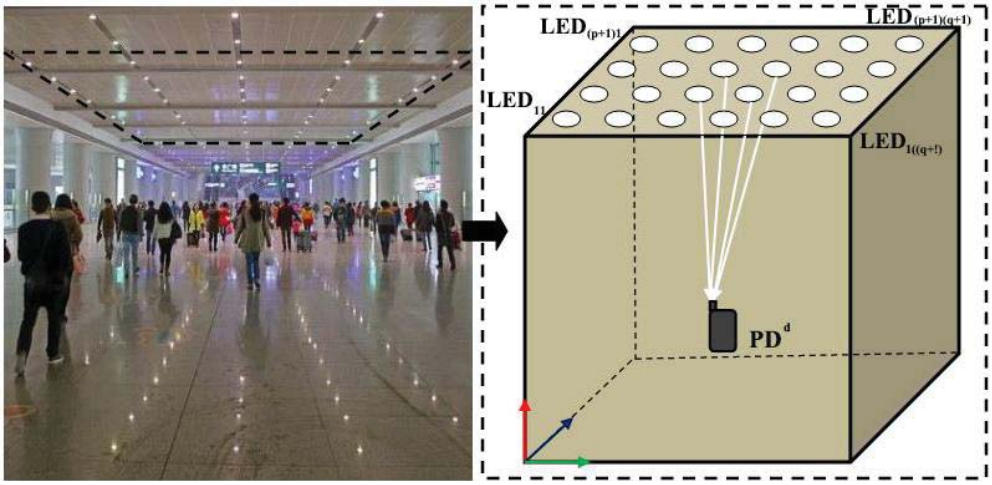
LED(p+1)1
LED(p+1)(q+1)
LED11
LED1((q+!)
PDd

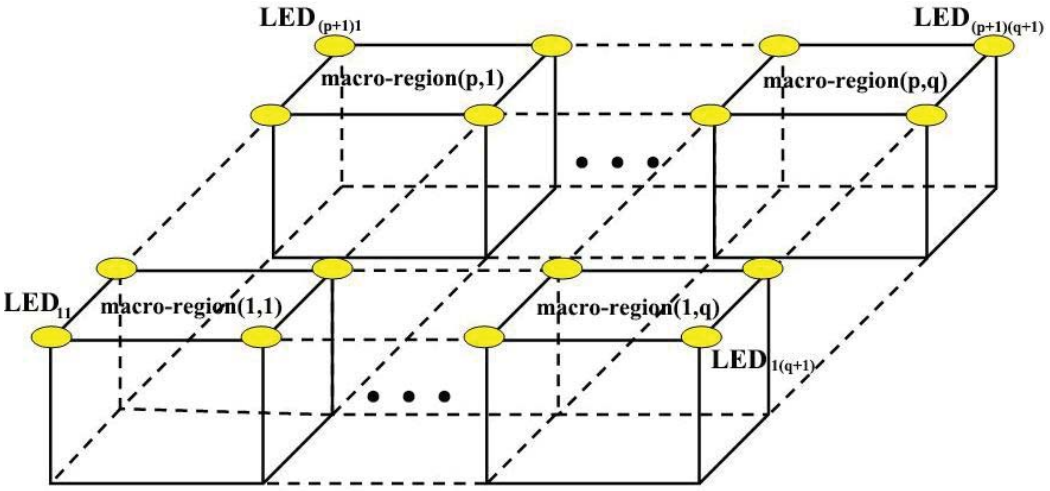
LED(p+1)1
LED(p+1)(q+1)
macro-region(p,1)
macro-region(p,q)
LED11
macro-region(1,1)
macro-region(1,q)
LED1(q+1)

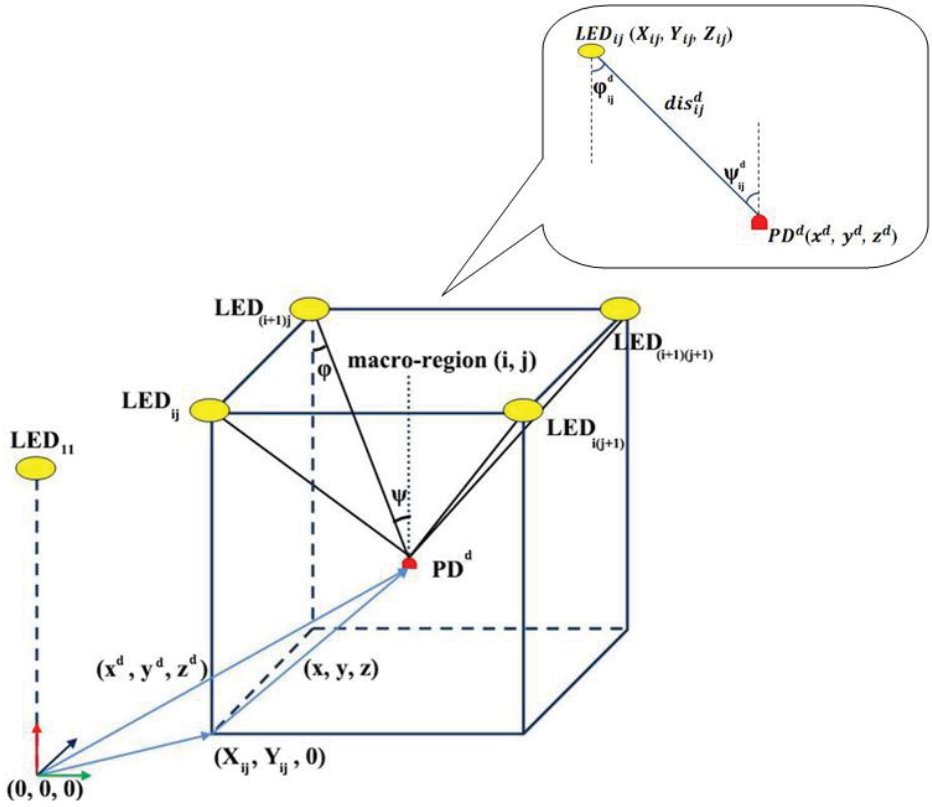
LED_ij (X_ij, Y_ij, Z_ij)
φ^d_ij
dis^d_ij
ψ^d_ij
PD^d(x^d, y^d, z^d)
LED_(i+1)j
LED_(i+1)(j+1)
macro-region (i, j)
φ
LED_ij
LED_i(j+1)
LED_11
ψ
PD^d
(x^d, y^d, z^d)
(x, y, z)
(X_ij, Y_ij, 0)
(0, 0, 0)

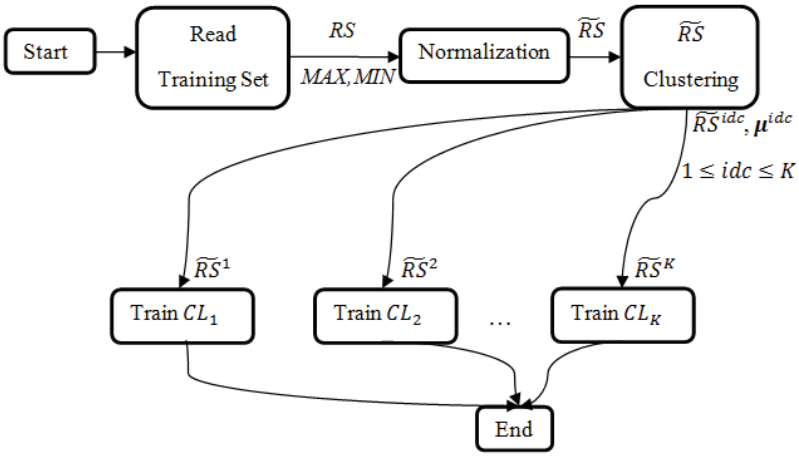
Start
Read
Training Set
RS
MAX, MIN
Normalization
$\widetilde{RS}$
$\widetilde{RS}$
Clustering
$\widetilde{RS}^{idc}, \boldsymbol{\mu}^{idc}$
$1 \leq idc \leq K$
$\widetilde{RS}^1$
$\widetilde{RS}^2$
$\widetilde{RS}^K$
Train CL_1
Train CL_2
...
Train CL_K
End

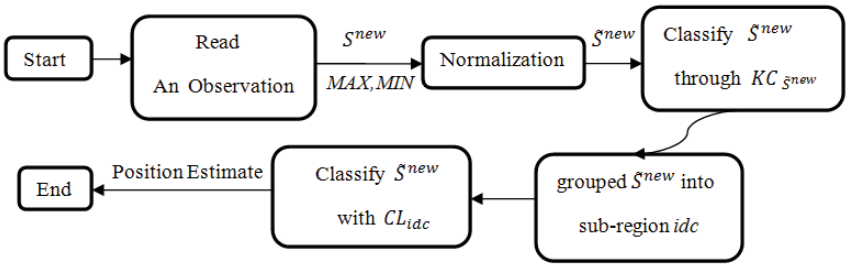
Start
Read
An Observation
S^{new}
MAX, MIN
Normalization
S^{new}
Classify S^{new}
through $KC_{S^{new}}$
grouped S^{new} into
sub-region idc
Classify S^{new}
with CL_{idc}
Position Estimate
End

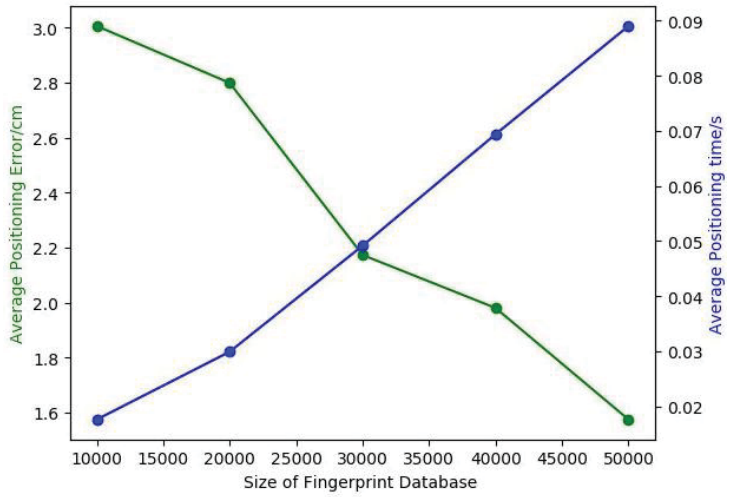
Average Positioning Error/cm
Average Positioning time/s
Size of Fingerprint Database
3.0
2.8
2.6
2.4
2.2
2.0
1.8
1.6
0.09
0.08
0.07
0.06
0.05
0.04
0.03
0.02
10000
15000
20000
25000
30000
35000
40000
45000
50000

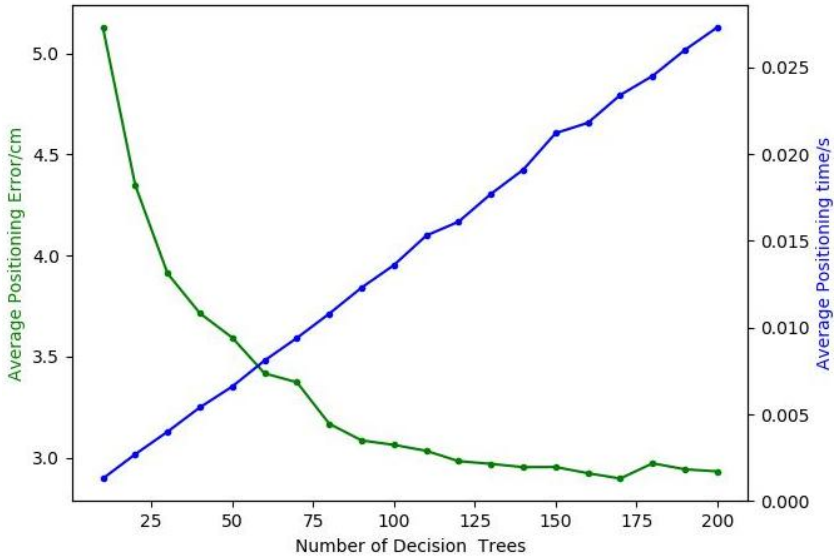
Average Positioning Error/cm
Average Positioning time/s
Number of Decision Trees
5.0
4.5
4.0
3.5
3.0
0.025
0.020
0.015
0.010
0.005
0.000
25
50
75
100
125
150
175
200

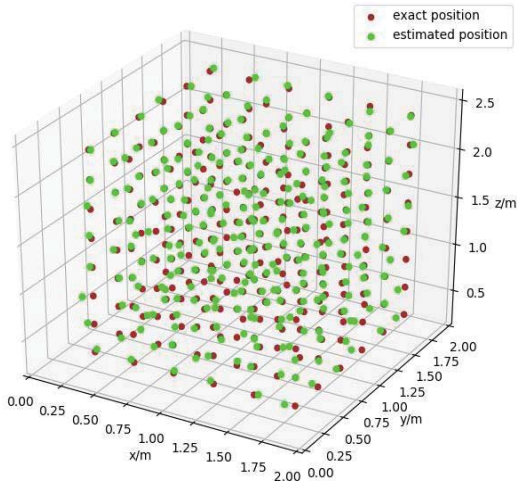
exact position
estimated position
2.5
2.0
1.5
z/m
1.0
0.5
2.00
1.75
1.50
1.25
1.00
0.75
y/m
0.50
0.25
0.00
0.00
0.25
0.50
0.75
1.00
1.25
1.50
1.75
2.00
x/m

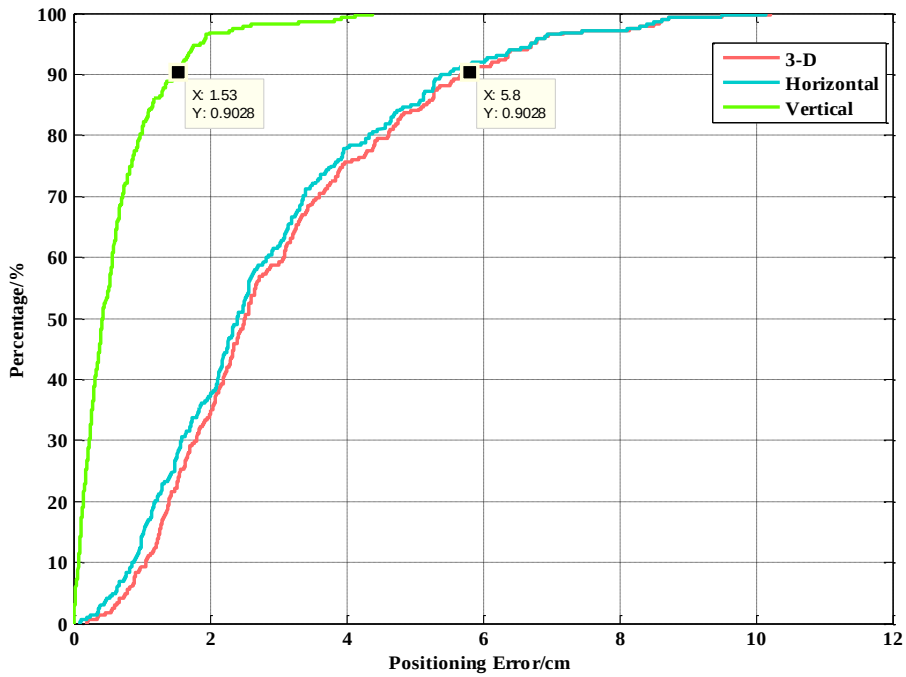
100
90
80
70
60
50
40
30
20
10
0
Percentage/%
0
2
4
6
8
10
12
Positioning Error/cm
X: 1.53
Y: 0.9028
X: 5.8
Y: 0.9028
3-D
Horizontal
Vertical

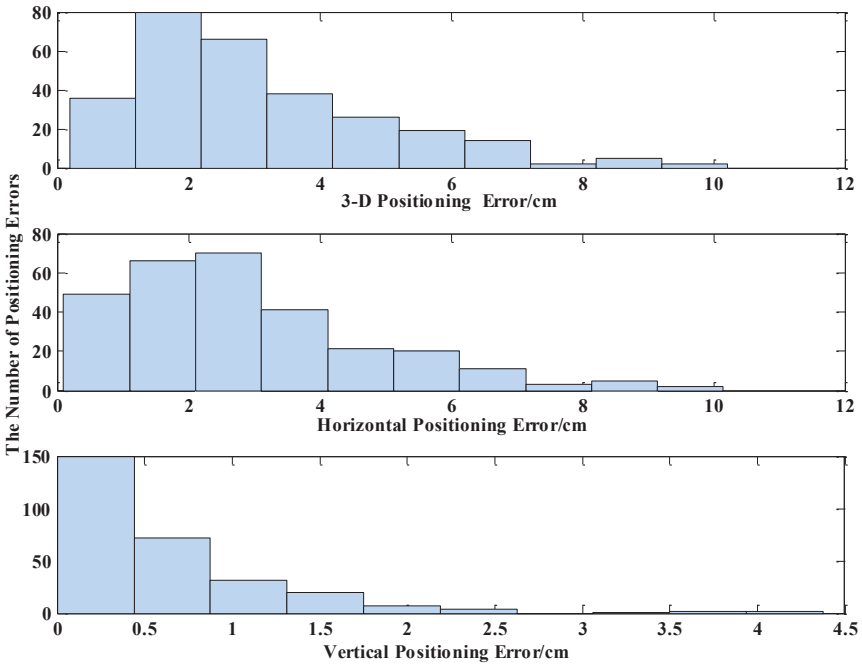
The Number of Positioning Errors
3-D Positioning Error/cm
Horizontal Positioning Error/cm
Vertical Positioning Error/cm

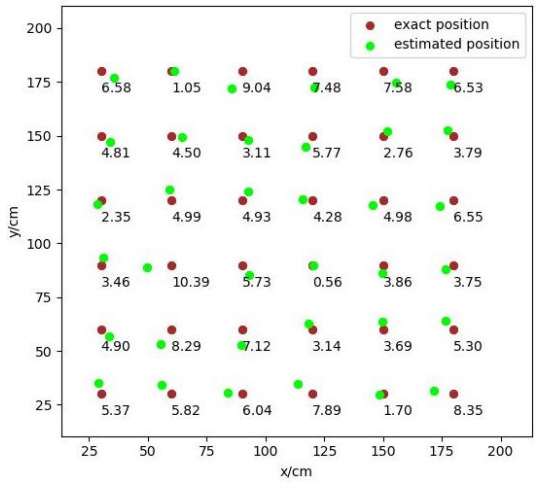
exact position
estimated position
6.58 1.05 9.04 7.48 7.58 6.53
4.81 4.50 3.11 5.77 2.76 3.79
2.35 4.99 4.93 4.28 4.98 6.55
3.46 10.39 5.73 0.56 3.86 3.75
4.90 8.29 7.12 3.14 3.69 5.30
5.37 5.82 6.04 7.89 1.70 8.35
y/cm
x/cm

(a)

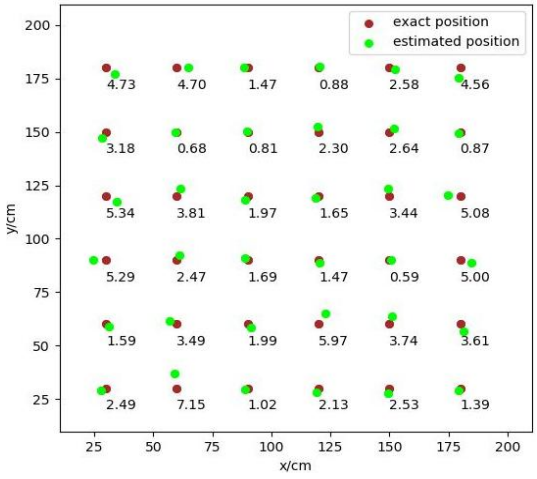
exact position
estimated position
4.73 4.70 1.47 0.88 2.58 4.56
3.18 0.68 0.81 2.30 2.64 0.87
5.34 3.81 1.97 1.65 3.44 5.08
5.29 2.47 1.69 1.47 0.59 5.00
1.59 3.49 1.99 5.97 3.74 3.61
2.49 7.15 1.02 2.13 2.53 1.39
y/cm
x/cm

(b)

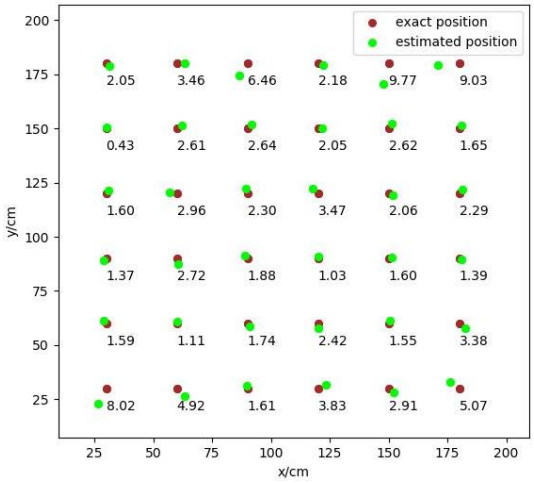
exact position
estimated position
2.05 3.46 6.46 2.18 9.77 9.03
0.43 2.61 2.64 2.05 2.62 1.65
1.60 2.96 2.30 3.47 2.06 2.29
1.37 2.72 1.88 1.03 1.60 1.39
1.59 1.11 1.74 2.42 1.55 3.38
8.02 4.92 1.61 3.83 2.91 5.07
y/cm
x/cm

(c)

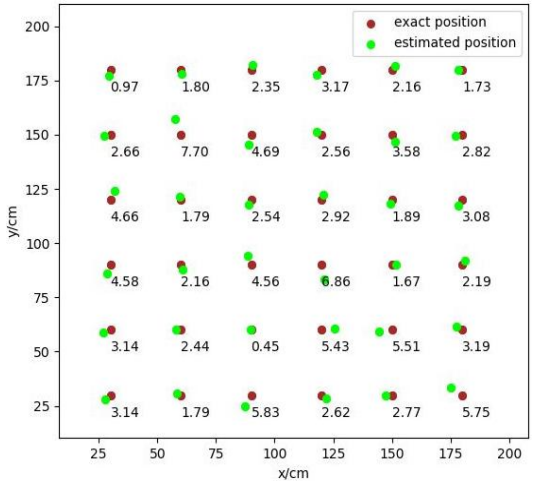
exact position
estimated position
0.97 1.80 2.35 3.17 2.16 1.73
2.66 7.70 4.69 2.56 3.58 2.82
4.66 1.79 2.54 2.92 1.89 3.08
4.58 2.16 4.56 6.86 1.67 2.19
3.14 2.44 0.45 5.43 5.51 3.19
3.14 1.79 5.83 2.62 2.77 5.75
y/cm
x/cm

(d)

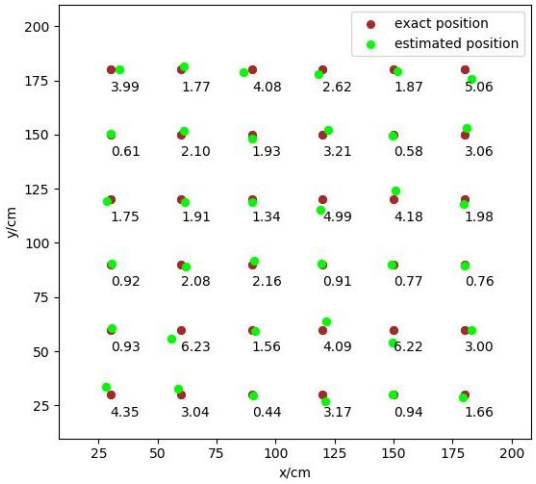
exact position
estimated position
3.99 1.77 4.08 2.62 1.87 5.06
0.61 2.10 1.93 3.21 0.58 3.06
1.75 1.91 1.34 4.99 4.18 1.98
0.92 2.08 2.16 0.91 0.77 0.76
0.93 6.23 1.56 4.09 6.22 3.00
4.35 3.04 0.44 3.17 0.94 1.66
y/cm
x/cm

(e)

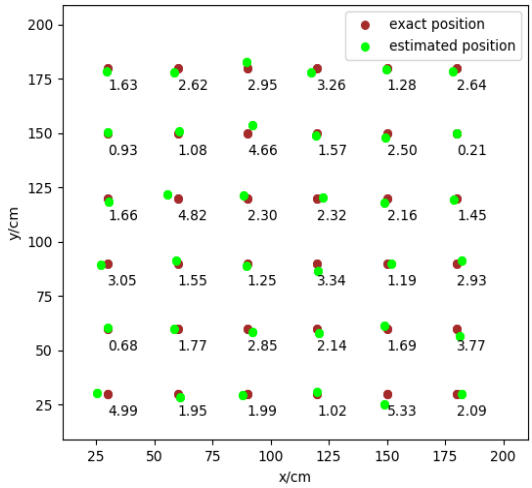
exact position
estimated position
1.63 2.62 2.95 3.26 1.28 2.64
0.93 1.08 4.66 1.57 2.50 0.21
1.66 4.82 2.30 2.32 2.16 1.45
3.05 1.55 1.25 3.34 1.19 2.93
0.68 1.77 2.85 2.14 1.69 3.77
4.99 1.95 1.99 1.02 5.33 2.09
y/cm
x/cm

(f)

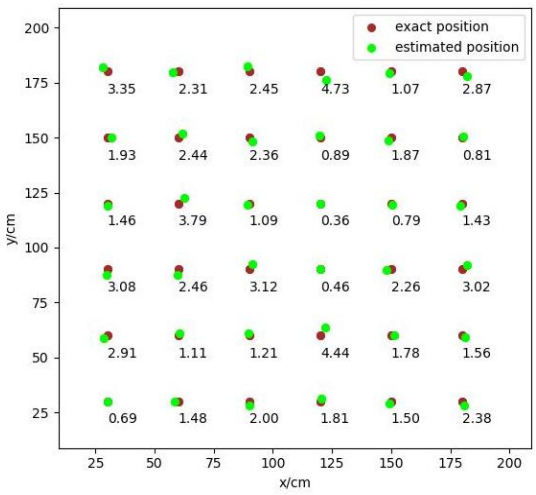
exact position
estimated position
y/cm
x/cm
3.35 2.31 2.45 4.73 1.07 2.87
1.93 2.44 2.36 0.89 1.87 0.81
1.46 3.79 1.09 0.36 0.79 1.43
3.08 2.46 3.12 0.46 2.26 3.02
2.91 1.11 1.21 4.44 1.78 1.56
0.69 1.48 2.00 1.81 1.50 2.38

(g)

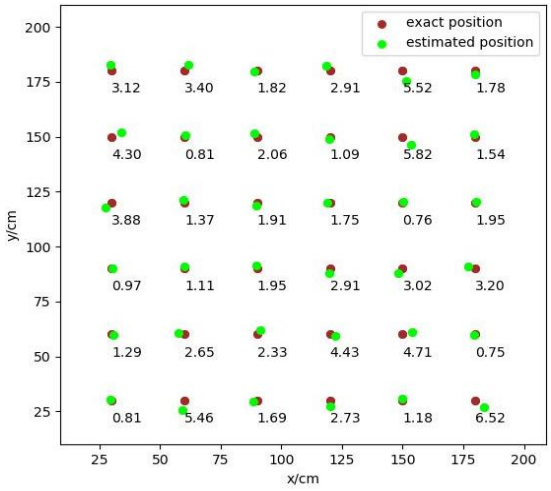
exact position
estimated position
y/cm
x/cm
3.12 3.40 1.82 2.91 5.52 1.78
4.30 0.81 2.06 1.09 5.82 1.54
3.88 1.37 1.91 1.75 0.76 1.95
0.97 1.11 1.95 2.91 3.02 3.20
1.29 2.65 2.33 4.43 4.71 0.75
0.81 5.46 1.69 2.73 1.18 6.52

(h)

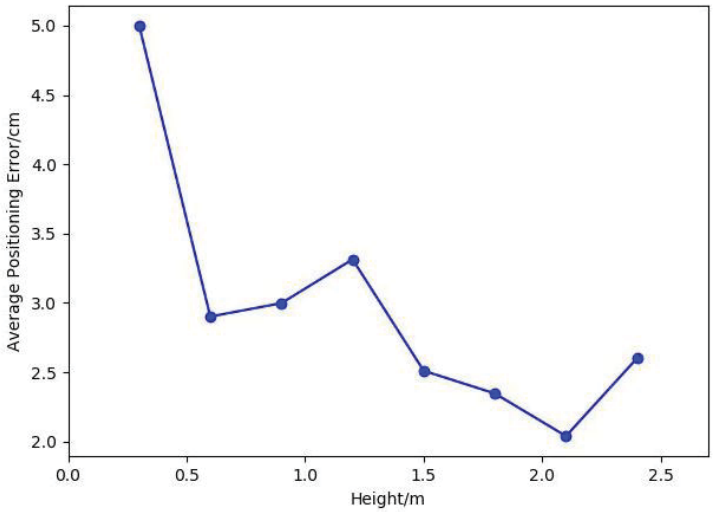
Average Positioning Error/cm
5.0
4.5
4.0
3.5
3.0
2.5
2.0
0.0
0.5
1.0
1.5
2.0
2.5
Height/m

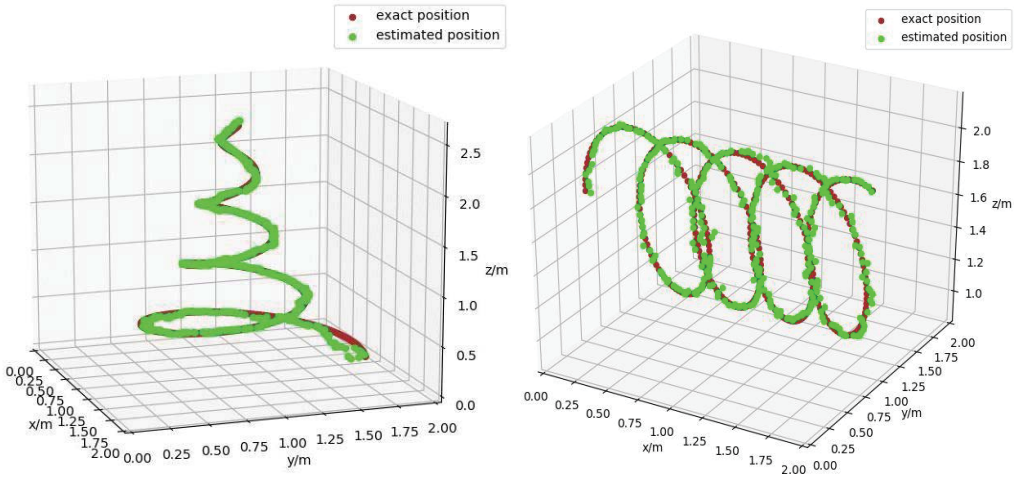
exact position
estimated position
z/m
x/m
y/m
exact position
estimated position
z/m
x/m
y/m

(a) (b)

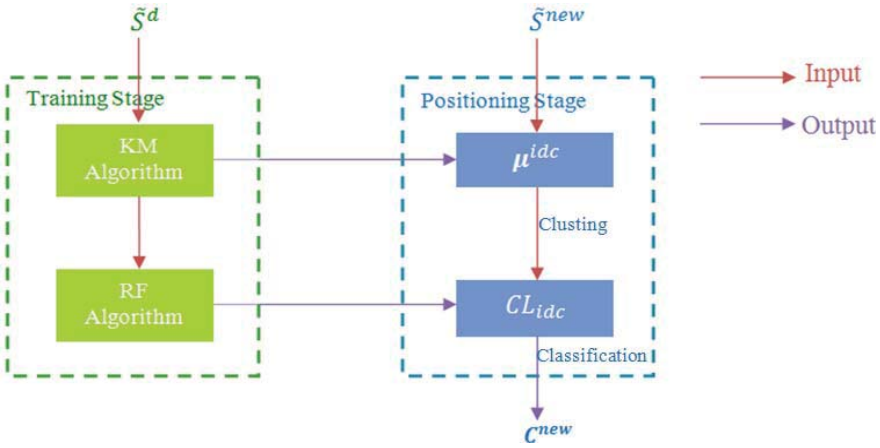
$\tilde{S}^{d}$
$\tilde{S}^{new}$
Input
Output
Training Stage
KM Algorithm
RF Algorithm
Positioning Stage
μ^{idc}
Clusting
CL_{idc}
Classification
C^{new}

Algorithm 1 K-Means Clustering

Training Stage:
Input: K, $\tilde{S}^d$, $\tilde{\boldsymbol{S}}^{idc}$
Output: $\boldsymbol{\mu}^{idc}$
1: Create K points as the initial centroid by random selection
2: **for** $\tilde{S}^d$ such that $1 \le d \le D$ do
3: **for** $\tilde{\boldsymbol{S}}^{idc}$ such that $1 \le idc \le K$ do
4: Calculate Euclidean distance between $\tilde{S}^d$ and $\tilde{\boldsymbol{S}}^{idc}$
5: **end for**
6: Group $\tilde{S}^d$ into cluster with $\min(ED(\tilde{S}^d, \tilde{\boldsymbol{S}}^{idc}))$
7: **end for**
8: **for** $1 \le idc \le K$ do
9: $\boldsymbol{\mu}^{idc} \leftarrow$ arithmetic mean of $\tilde{S}^d$ of cluster idc
10: **end for**
Positioning Stage:
Input: $\tilde{S}^{new}$, $\boldsymbol{\mu}^{idc}$
Output: $KC_{\tilde{S}^{new}}$
1: **for** $1 \le idc \le K$ do
2: Group $\tilde{S}^{new}$ into cluster with $\min(ED(\tilde{S}^d, \boldsymbol{\mu}^{idc}))$
3: **end for**

Algorithm 2 Random Forest Classification

Training Stage:
Input: $\widetilde{RS}_{idc}$, Z, P, p
Output: CL_{idc}
1: **for** $1 \le \varepsilon \le ntree$ do
2: Draw a bootstrap sample Z^* of size N from the training data
3: Grow a random-forest tree T_ε to the bootstrapped data
4: **do**
5: **for** each terminal node for the tree
6: Select m variables at random from p variables
7: Pick the best variable/spilt-point from the m
8: Spilt the node into two daughter nodes
9: **end for**
10: **while** minimum leaf node size and maximum tree depth are not reached
11: **end for**
12: $CL_{idc} \leftarrow$ ensemble of T_ε
Positioning Stage:
Input: $\tilde{S}^{new}$, CL_{idc}
Output: C^{new}
1: **for** $1 \le idc \le K$ do
2: Choose the idp with max($Conf_{idc}$)
3: **end for**

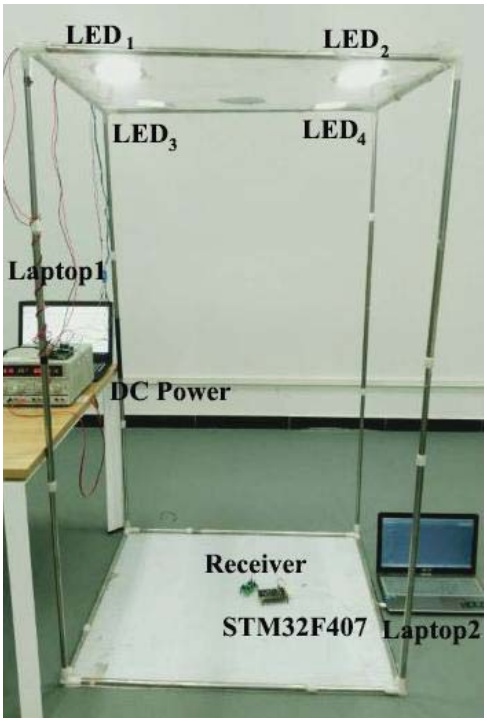
LED 1
LED 2
LED 3
LED 4
Laptop1
DC Power
Receiver
STM32F407
Laptop2

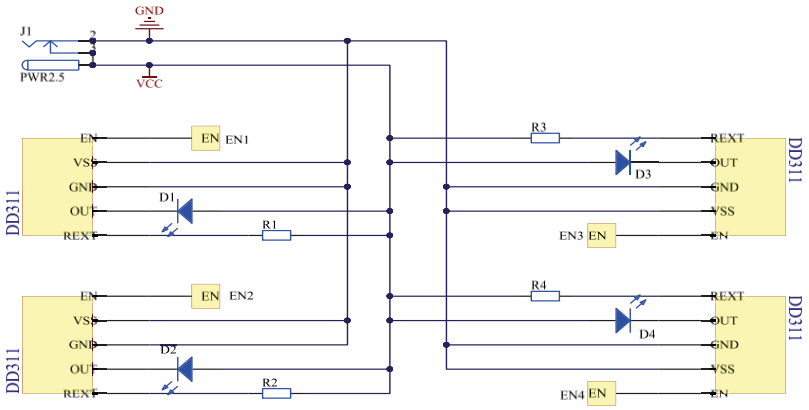
GND
J1
2
PWR2.5
VCC
EN
VSS
GND
OUT
REXT
DD311
EN EN1
D1
R1
EN EN2
D2
R2
R3
D3
R4
D4
REXT
OUT
GND
VSS
EN
EN3 EN
EN4 EN

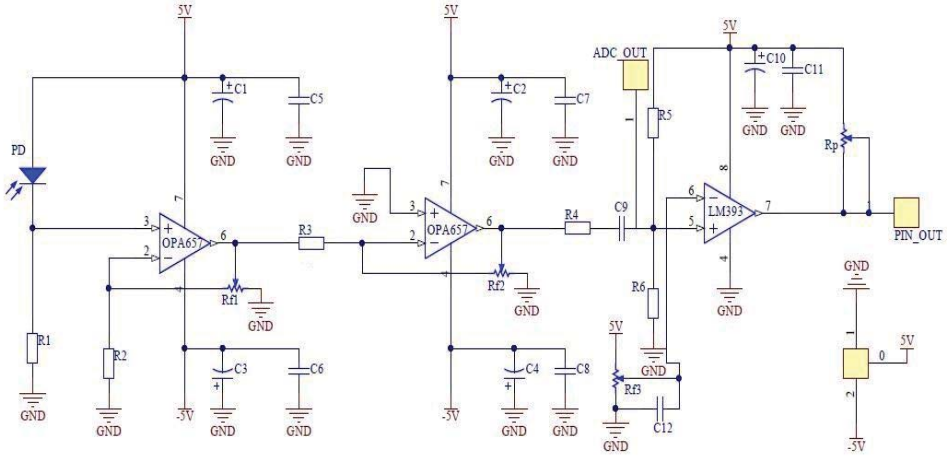
5V
PD
C1
C5
GND
OPA657
R3
Rf1
R1
R2
-5V
C3
C6
C2
C7
R4
Rf2
C4
C8
ADC_OUT
R5
C9
R6
Rf3
C12
C10
C11
LM393
Rp
PIN_OUT
0

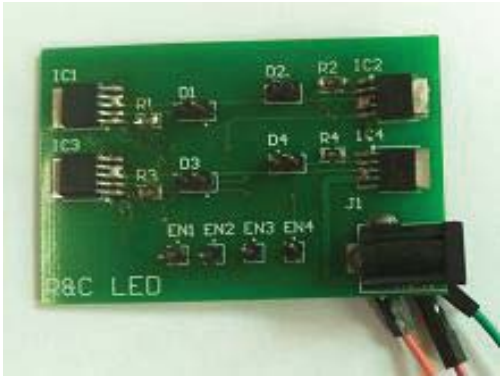
IC1
R1
D1
D2
R2
IC2
IC3
R3
D3
D4
R4
IC4
J1
EN1 EN2 EN3 EN4
P&C LED


C1
C2
C10
Rp
C5
U3
C7
U2
R4
C9
R11
C3
R12
C4
R13
+5L
GND
+5V

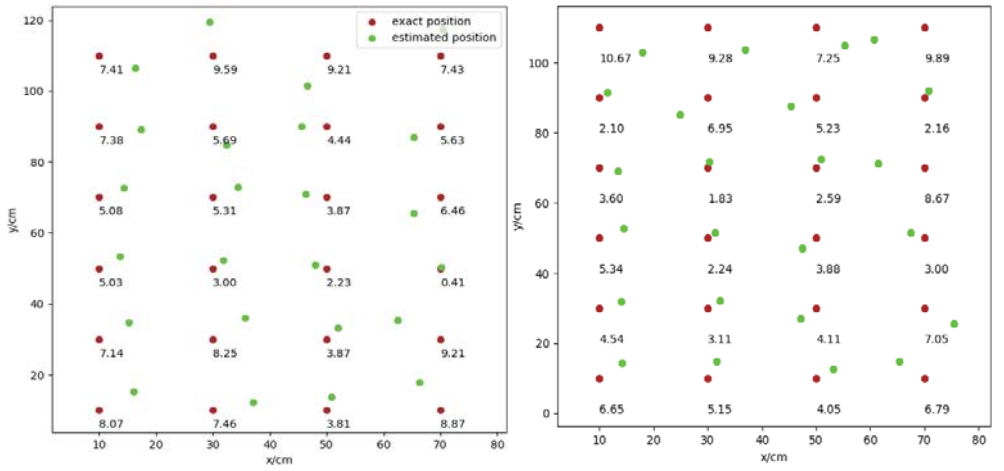
exact position
estimated position
7.41 9.59 9.21 7.43
7.38 5.69 4.44 5.63
5.08 5.31 3.87 6.46
5.03 3.00 2.23 0.41
7.14 8.25 3.87 9.21
8.07 7.46 3.81 8.87
10.67 9.28 7.25 9.89
2.10 6.95 5.23 2.16
3.60 1.83 2.59 8.67
5.34 2.24 3.88 3.00
4.54 3.11 4.11 7.05
6.65 5.15 4.05 6.79
y/cm
x/cm

(a) (b)

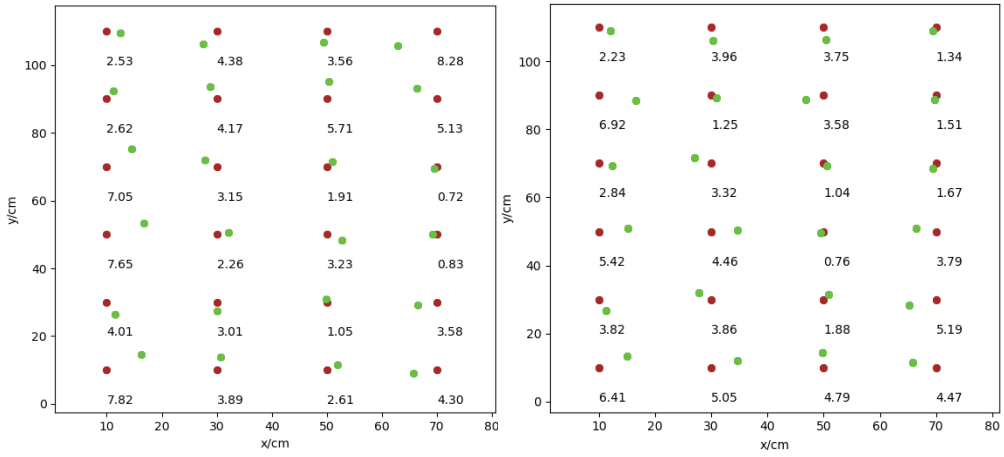
2.53 4.38 3.56 8.28
2.62 4.17 5.71 5.13
7.05 3.15 1.91 0.72
7.65 2.26 3.23 0.83
4.01 3.01 1.05 3.58
7.82 3.89 2.61 4.30
2.23 3.96 3.75 1.34
6.92 1.25 3.58 1.51
2.84 3.32 1.04 1.67
5.42 4.46 0.76 3.79
3.82 3.86 1.88 5.19
6.41 5.05 4.79 4.47
y/cm
x/cm

(c) (d)

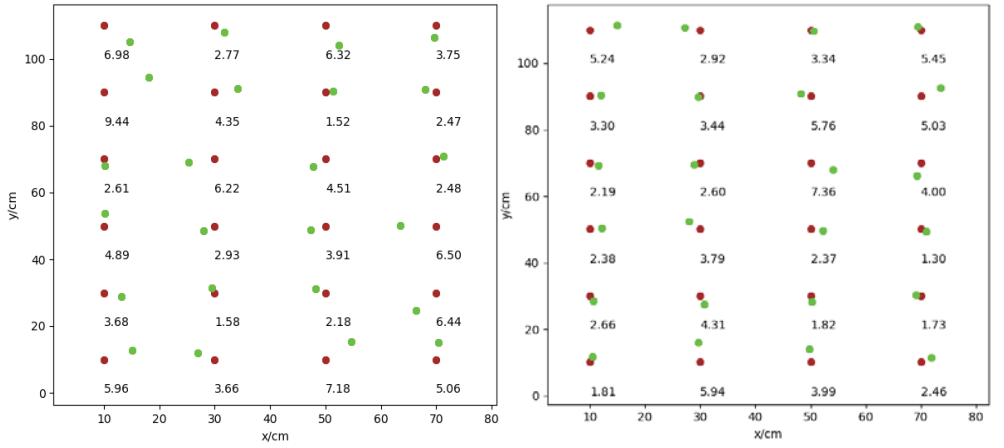
6.98 2.77 6.32 3.75
9.44 4.35 1.52 2.47
2.61 6.22 4.51 2.48
4.89 2.93 3.91 6.50
3.68 1.58 2.18 6.44
5.96 3.66 7.18 5.06
5.24 2.92 3.34 5.45
3.30 3.44 5.76 5.03
2.19 2.60 7.36 4.00
2.38 3.79 2.37 1.30
2.66 4.31 1.82 1.73
1.81 5.94 3.99 2.46
y/cm
x/cm

(e) (f)

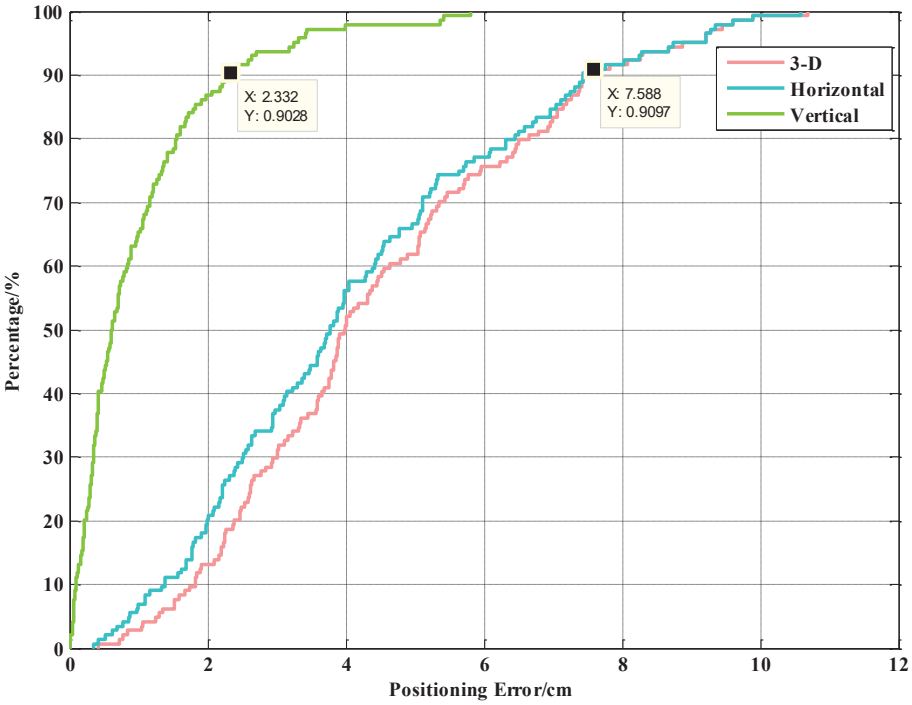
100
90
80
70
60
50
40
30
20
10
0
0
2
4
6
8
10
12
Percentage/%
Positioning Error/cm
X: 2.332
Y: 0.9028
X: 7.588
Y: 0.9097
3-D
Horizontal
Vertical

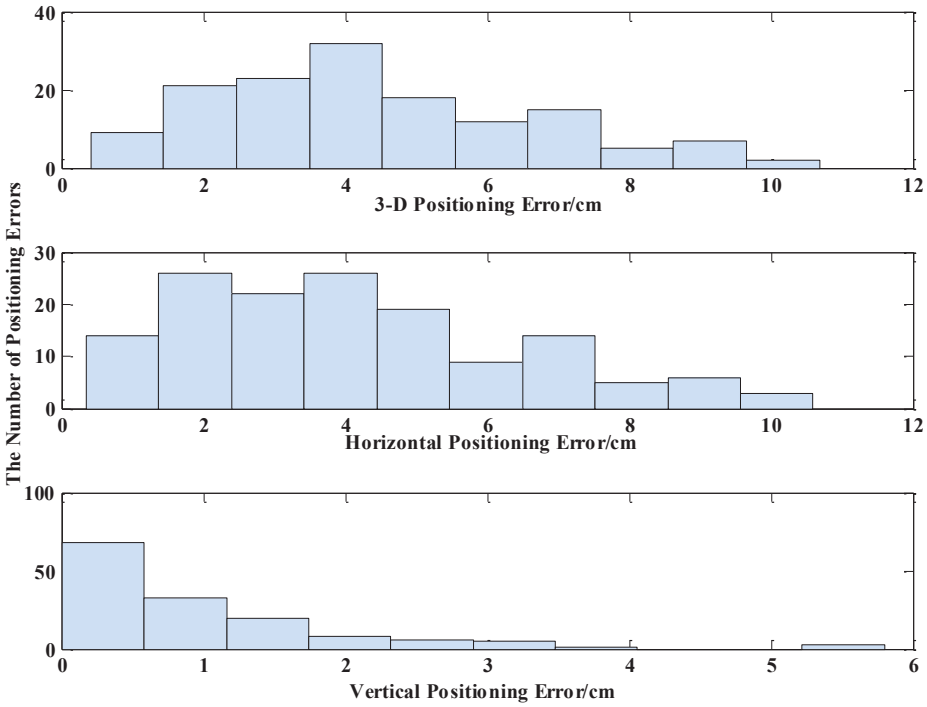
The Number of Positioning Errors
3-D Positioning Error/cm
Horizontal Positioning Error/cm
Vertical Positioning Error/cm